

Karlsruher Institut für Technologie
Institut für Theoretische Physik

Diplomarbeit

Colour Charge Effects in Hadronization

Farbladungseffekte in der Hadronisierung

Christian Röhr

Mai 2010

Referent: Prof. Dr. D. Zeppenfeld

Korreferent: Prof. Dr. G. Quast

Last modified: July 7, 2010

Ich versichere, dass ich diese Arbeit selbstständig verfasst und keine anderen als die angegebenen Hilfsmittel benutzt habe.

Christian Röhr
Karlsruhe, den 3. Mai 2010

Als Diplomarbeit anerkannt.

Prof. Dr. Dieter Zeppenfeld
Karlsruhe, den 3. Mai 2010

Contents

1	Introduction	1
2	Quantum Chromodynamics	3
2.1	The QCD Lagrangian	3
2.2	Asymptotic freedom and confinement	4
2.3	Parton shower approximation	5
2.3.1	Parton branching in the collinear limit	5
2.3.2	Branching cascade	6
2.3.3	Colour coherence	7
2.4	Excursus: Standard Model	7
3	Event generation with Herwig++	11
3.1	Outline	11
3.2	Hard process	11
3.3	Parton shower	12
3.3.1	Initial showering conditions	12
3.3.2	Final-state radiation	12
3.3.3	Initial-state radiation	13
3.3.4	Colour flow	13
3.4	Hadronization	13
3.4.1	Non-perturbative gluon splitting and cluster formation	14
3.4.2	Cluster fission and decay	14
3.5	Underlying event simulation	14
3.5.1	Multiple interactions	15
3.5.2	Soft interactions	16
4	Colour reconnection	17
4.1	Kinematics	17
4.2	Overlap in spacetime and soft gluon exchange	17
4.3	Perturbative colour reconnection	18
4.4	Non-perturbative colour reconnection	18
4.5	Sensitive observables	19
4.5.1	Particle flow at LEP2	19
4.5.2	Underlying event at the Tevatron	19
5	Implementation in Herwig++	21
5.1	Spacetime model	21
5.1.1	Distribution of scattering centres	21
5.1.2	Lifelong generation	22

5.1.3	Combining the sub-models	24
5.1.4	Plausibility check	25
5.2	Colour reconnection model	27
5.2.1	Introduction	27
5.2.2	Algorithm	27
5.2.3	Colour octet veto	29
5.2.4	Cluster mass distribution	29
6	Particle flow in WW events	31
6.1	Analysis details	31
6.1.1	Hard process	31
6.1.2	Event selection	32
6.1.3	Identification of jet pairs	34
6.1.4	Definition of inter-jet regions	37
6.1.5	Assignment of particles to inter-jet regions	37
6.2	Expected results	38
6.3	Particle flow distribution	38
6.4	Particle flow ratio	40
6.5	Summary	40
6.6	Model investigation	40
6.6.1	Initial parton shower evolution scale	40
6.6.2	A momentum space based model	42
6.6.3	Random colour reconnection	44
7	Outlook: Underlying event at the Tevatron	47
7.1	Introduction	47
7.2	Colour connections in hadron collisions	47
7.3	Underlying event in $p\bar{p}$ collisions at 1.8 TeV	48
7.3.1	The “transverse” region	49
7.3.2	Dependency on the hadron radius	49
7.3.3	Momentum-space colour reconnection	49
7.3.4	Conclusion	50
8	Summary and conclusions	53
A	Sampling of scattering centres	55
B	Lifetime of virtual partons	57
C	Model parameters	59
	Zusammenfassung	65
	Danksagung	69

1 Introduction

Monte Carlo event generators play a crucial part in collider physics. They are used for the simulation of final states in particle collisions which can be compared to data measured in experiments. Large parts of the event generation are based on Quantum Chromodynamics (QCD), which is the theory of strong interactions. This theory is formulated in terms of quarks, antiquarks and gluons, collectively referred to as partons.

For the calculation of scattering amplitudes in high-energy physics, perturbation theory can be used. This technique provides the possibility of generating scattering processes on a probabilistic basis. However, the final-state particles of these hard processes cannot be observed directly, if there are partons amongst them. They do not exist as free particles, but are only observed in bound states, called hadrons. This remarkable feature of QCD is called *confinement*.

The transition from the partonic final state of the hard process to a final state consisting of observable hadrons is handled by event generators in two parts. In the first step, so-called *parton showers* are generated, which derive from a careful treatment of perturbative QCD. At the end of this procedure, where perturbation theory ceases to be valid, a set of low-scale partons remains. In the second step, *hadronization models* are utilized in order to transform the partonic state to a hadronic final state. Existing hadronization models can be regarded as phenomenological prescriptions that try to yield a reliable simulation of experimental findings.

This work aims at the implementation and investigation of a so-called *colour reconnection* (CR) model in the Monte Carlo event generator **Herwig++** [1]. The model can be regarded as an extension to **Herwig++**'s default hadronization model. It takes account of possible effects caused by the exchange of additional soft gluons during the non-perturbative hadronization phase. The CR model is designed to be applicable to both lepton and hadron collisions. It is inspired by an existing implementation in **Herwig++**'s predecessor, **HERWIG** [2].

Chapter 2 recapitulates the foundations of Quantum Chromodynamics and gives a brief overview of the Standard Model of particle physics. Moreover, the concept of parton showers is introduced in order to prepare for Chapter 3, which outlines the functionality of **Herwig++**.

The concept of colour reconnection is explained in Chapter 4. This serves as a basis for the CR model which has been implemented in **Herwig++**. The implementation is depicted in Chapter 5.

In Chapter 6 the colour reconnection model is tested against data from the *Large Electron-Positron Collider* (LEP). In particular, the particle flow in hadronic W pair decays is analyzed. This observable is expected to be sensitive to colour reconnection.

Finally, Chapter 7 gives an outlook on the impact of colour reconnection on observables that are related to the so-called underlying event in hadron collisions. Conclusions follow in Chapter 8.

2 Quantum Chromodynamics

The formation of hadrons in particle collisions is not understood from first principles. It happens at small energy scales, where perturbative QCD breaks down. The colour reconnection model studied in this work applies exactly during this phase. This chapter serves as an introduction to Quantum Chromodynamics, which event generation is built upon. The focus is on a depiction of the running coupling as well as on the description of parton showers. Finally, the introduction of the nowadays established theory of particle physics is completed in a brief discussion of the Standard Model.

2.1 The QCD Lagrangian

The theory of strong interactions is a non-abelian gauge theory based on the $SU(3)_C$ gauge group. The classical QCD Lagrangian is

$$\mathcal{L}_{\text{QCD}} = \sum_{\Psi=u,d,s,\dots} \bar{\Psi}(i\gamma^\mu D_\mu - m_\Psi)\Psi - \frac{1}{4}F^{a\mu\nu}F_{\mu\nu}^a, \quad (2.1)$$

with the covariant derivative

$$D_\mu = \partial_\mu - ig_s T^a G_\mu^a. \quad (2.2)$$

Ψ are the massive quark fields. They transform according to the fundamental representation of $SU(3)$, *i.e.* are (colour) triplets, $\Psi = (\Psi_1, \Psi_2, \Psi_3)$.

$$F_{\mu\nu}^a = \partial_\mu G_\nu^a - \partial_\nu G_\mu^a + g_s f^{abc} G_\mu^b G_\nu^c \quad (2.3)$$

are the field strength tensors of the eight massless gluons G_μ^a in the adjoint representation of $SU(3)$, corresponding to the eight $SU(3)$ generators T^a . g_s is the strong coupling constant. The structure constants f^{abc} are defined by the commutation relations,

$$[T^a, T^b] = if^{abc}T^c, \quad (2.4)$$

of the $SU(3)$ generators. In the fundamental representation of $SU(3)$, the generators are the Gell-Mann matrices, $T_{ij}^a = \frac{\lambda_{ij}^a}{2}$.

Note that the explicit introduction of fermion mass terms $m\bar{\Psi}\Psi$ in \mathcal{L}_{QCD} is possible if we treat QCD as a separate theory. However, in the Standard Model, which includes the theory of electroweak interactions, these terms break the weak isospin and hypercharge symmetries (*cf.* Sec. 2.4).

\mathcal{L}_{QCD} is constructed to be invariant under infinitesimal local $SU(3)$ gauge transformations

$$\begin{aligned}\Psi(x) &\rightarrow [1 + ig_s\theta^a(x)T^a] \Psi(x), \\ G_\mu^a(x) &\rightarrow G_\mu^a(x) + \partial_\mu\theta^a(x) - g_s f^{abc}\theta^b(x)G_\mu^c(x),\end{aligned}\tag{2.5}$$

where $\theta^a(x)$ are infinitesimal real parameters.

For the quantization of the gluon field, the freedom of gauge transformations (2.5) has to be eliminated by including a gauge-fixing term $\mathcal{L}_{\text{gauge}}$. Moreover, a further term $\mathcal{L}_{\text{ghost}}$ is required to cancel unphysical degrees of freedom. See e.g. Ref. [3] for details.

The first term in \mathcal{L}_{QCD} accounts for the kinetic energy of the quarks as well as the interaction of quarks with gluons. This interaction is flavour-diagonal, *i.e.* the quark flavour is not changed by the interaction with a gluon.

An important property of QCD is hidden in the term proportional to F^2 . It contains three-point and four-point gluon self-interactions terms (descending from terms proportional to G^3 and G^4). This leads to asymptotic freedom in QCD, which is introduced in the next section.

2.2 Asymptotic freedom and confinement

QCD has the property of *asymptotic freedom* [4, 5], which means that the QCD coupling $\alpha_s = g_s^2/4\pi$ becomes small at high energies or short distances. This scale dependence of α_s manifests in the β function

$$\beta(\alpha_s) = Q^2 \frac{\partial\alpha_s}{\partial Q^2}.\tag{2.6}$$

Q is the energy scale where the coupling is measured. In QCD, β can be expanded in powers of α_s ,

$$\beta(\alpha_s) = -b\alpha_s^2(1 + b'\alpha_s + \mathcal{O}(\alpha_s^2)),\tag{2.7}$$

with $b = \frac{33-2n_f}{12\pi}$ and $b' = \frac{153-19n_f}{2\pi(33-2n_f)}$. n_f is the number of quark flavours with mass smaller than $\sim Q$. The expansion coefficients are calculated via quantum corrections to the bare vertices of the theory [6].

β is negative since in QCD the number of quark flavours is limited to 6. The negative sign of β and thus asymptotic freedom can be traced back to the existence of a three-gluon coupling term in the QCD Lagrangian (2.1) [3]. The strong coupling decreases with increasing energy and therefore becomes small for short-distance interactions.

At 1-loop order, *i.e.* if only the leading term in Eq. (2.7) is regarded, the running coupling can be expressed as

$$\alpha_s(Q^2) = \frac{\alpha_s(\mu^2)}{1 + \frac{\alpha_s(\mu^2)}{12\pi}(33 - 2n_f) \log(Q^2/\mu^2)}.\tag{2.8}$$

μ is a parameter with energy dimension 1, which has to be chosen during the renormalization program, necessary for the cancellation of ultra-violet divergences. To quote values for α_s , a typical choice for this scale is the Z^0 mass, $\mu^2 = M_Z^2$. The coupling at this scale has been measured to be $\alpha_s(M_Z^2) \approx 0.12$.

Eq. (2.8) shows that the coupling becomes large at sufficiently low Q^2 . The scale where this happens is

$$\Lambda^2 = \mu^2 \exp \left[\frac{-12\pi}{(33 - 2n_f)\alpha_s(\mu^2)} \right], \quad (2.9)$$

which has been measured to be $\Lambda \approx 200$ MeV. Perturbative QCD in terms of quarks and gluons is valid for Q^2 values much larger than Λ^2 . For small Q^2 of the order of Λ^2 , an expansion of an observable in α_s becomes unreasonable, *i.e.* perturbation theory breaks down.

The phenomenon that quarks and gluons are not observed as states which propagate over macroscopic distances, is called (*colour*) *confinement*. Using lattice gauge theory, it can be shown that QCD provides this property [7]. In the case of sufficiently strong coupling, $SU(3)_C$ singlet states, *i.e.* the observed mesons and baryons, are the only possible finite-energy states.

2.3 Parton shower approximation

In perturbative QCD, hard processes are usually calculated to fixed order in α_s . In principle, higher accuracy for each process can be achieved by including corrections to further orders in perturbation theory. These corrections, however, can be quite difficult and usually grow in complexity with increasing order of α_s . On top, in some cases the cross section for certain phase space regions of the final state is enhanced in higher orders [6], making fixed-order predictions unreliable.

It can be shown – for most hard processes at colliders – that QCD matrix elements exhibit enhancements for two kinematic configurations [6]:

1. The emission of a *soft* gluon
2. and the splitting of a gluon or light quark into two almost *collinear* partons.

In both cases the cross section σ_{n+1} for $n + 1$ emitted particles can be calculated from the cross section without additional emission, σ_n . Parton shower algorithm use this fact to generate emissions iteratively, which leads to a cascade of partons.

2.3.1 Parton branching in the collinear limit

Collinear enhancements are approximated by contributions of parton branchings. Consider a branching $a \rightarrow bc$, where the incoming parton a is time-like,

$$t \equiv p_a^2 > 0.$$

The possible branchings in QCD are $g \rightarrow gg$, $g \rightarrow q\bar{q}$ and $q \rightarrow qg$.

In the collinear limit, *i.e.* for small angles ϑ between the splitting products, the virtuality t of the emitting parton can be expressed as

$$t \approx z(1-z)E_a^2\vartheta^2,$$

where $z = E_b/E_a$ is the energy fraction of parton b with respect to the total energy E_a .

The amplitude \mathcal{M}_{n+1} has a factor $1/t \propto 1/\vartheta^2$ from the propagator of a . The remaining components of the matrix element, however, are proportional to ϑ , yielding in common a $1/t$ singularity in the *squared* amplitude.

One finds that the cross section for $n+1$ particles can be expressed as

$$d\sigma_{n+1} = d\sigma_n \frac{dt}{t} dz \frac{\alpha_s}{2\pi} \hat{P}_{ba}(z), \quad (2.10)$$

where $\hat{P}_{ba}(z)$ are the unregularized *splitting functions*,

$$\begin{aligned} \hat{P}_{gg}(z) &= 3 \left[\frac{1-z}{z} + \frac{z}{1-z} + z(1-z) \right], \\ \hat{P}_{qg}(z) &= \frac{1}{2} [z^2 + (1-z)^2], \\ \hat{P}_{qq}(z) &= \frac{4}{3} \frac{1+z^2}{1-z}. \end{aligned}$$

2.3.2 Branching cascade

The factor multiplied to $d\sigma_n$ in Eq. (2.10),

$$d\mathcal{P}_{ba} = \frac{dt}{t} dz \frac{\alpha_s}{2\pi} \hat{P}_{ba}(z), \quad (2.11)$$

can be interpreted as the *probability* for the emission of parton c with momentum fraction in the range $[1-z, 1-z-dz]$, while the virtuality evolves from t to $t-dt$ [8].

Based on this, the probability for evolution between the scale t_0 and t *without* resolvable emission of type $a \rightarrow bc$, called the *Sudakov form factor*, can be derived to be

$$\Delta_{ba}(t, t_0) \equiv \exp \left[- \sum_b \int_{t_0}^t \frac{dt'}{t'} \int dz \frac{\alpha_s}{2\pi} \hat{P}_{ba}(z) \right]. \quad (2.12)$$

This function enables Monte Carlo parton showers to sample the scale t' for the next branching. Iteratively, a chain of parton emissions is generated in this way, where the virtuality decreases with each step,

$$t_0 \gg t_1 \gg t_2 \dots$$

Since every emitted parton can be split in turn, a cascade of partons emerges. The showering ceases at branches where the remaining phase space is insufficient for further branchings.

The previous discussion motivates the generation of parton showers initiated by time-like partons. It can be shown [6] that Eq. (2.10) also holds for space-like branchings, where a is an incoming particle, which emits a parton c before connecting to the n -particle amplitude. In this case, however, the Sudakov form factor contains the parton density functions in order to take account for the probability that a is a parton of a specific type.

2.3.3 Colour coherence

The previously described branching process requires important modifications. As stated above, there is also an enhancement for the emission of soft gluons from external lines of a Feynman graph. In particular, amplitudes for soft gluon radiation from *pairs* of colour-connected partons interfere [9–11].

There are regions in the phase space of the emitted gluon where the cross section vanishes. Let ϑ_{ij} denote the angle between the emitting partons, i and j . It can be shown that soft emissions happens in cones around i and j with opening angle ϑ_{ij} [6]. This implies that the angle between the emitting parton and the emitted gluon is necessarily smaller than ϑ_{ij} .

In Monte Carlo shower algorithms the contribution of soft gluon emission can be taken into account by imposing *angular ordering* in the showering sequence. For the first time, this was done in the shower algorithm from Ref. [12], which has been implemented in HERWIG [13].

2.4 Excursus: Standard Model

The Standard Model combines QCD and the theory of weak and electromagnetic interactions. Recall that the gauge group of QCD is $SU(3)_C$. An additional gauge group $SU(2)_L \times U(1)_Y$ is used to describe also the weak and electromagnetic interactions in terms of a gauge theory. The fermions in the theory are six quarks, arranged in three generations,

$$\begin{pmatrix} u \\ d \end{pmatrix}, \begin{pmatrix} c \\ s \end{pmatrix}, \begin{pmatrix} t \\ b \end{pmatrix},$$

as well as three generations of leptons,

$$\begin{pmatrix} \nu_e \\ e \end{pmatrix}, \begin{pmatrix} \nu_\mu \\ \mu \end{pmatrix}, \begin{pmatrix} \nu_\tau \\ \tau \end{pmatrix}.$$

The gauge bosons are the eight gluons from QCD,

$$g_1, \dots, g_8,$$

Tab. 2.1 Representations of fermions and the higgs field in the $SU(3)_C \times SU(2)_L \times U(1)_Y$ group. **1**, **2** and **3** denote singlet, doublet and triplet representations, respectively. The last column shows the eigenvalue of the hypercharge operator Y (see below).

Ψ	$SU(3)_C$	$SU(2)_L$	$U(1)_Y$
$Q_L = \begin{pmatrix} u_L \\ d_L \end{pmatrix}$	3	2	$\frac{1}{6}$
u_R	3	1	$\frac{2}{3}$
d_R	3	1	$-\frac{1}{3}$
$L = \begin{pmatrix} \nu_L \\ e_L \end{pmatrix}$	1	2	$-\frac{1}{2}$
ν_R	1	1	0
e_R	1	1	-1
ϕ	1	2	$\frac{1}{2}$

and the four (physical) electroweak bosons

$$\gamma, W^+, W^-, Z^0.$$

The three quark and lepton generations coincide in their representation in the $SU(3)_C \times SU(2)_L \times U(1)_Y$ gauge group. Thus the following discussion can be restricted to one generation. The theory equally applies to the other generations.

The representations of the fermions in the three gauge groups are shown in Tab. 2.1. Left-chiral projections of the fields, $\Psi_L \equiv \frac{1}{2}(1 - \gamma_5)\Psi$, are in the fundamental representation of $SU(2)_L$. They build up weak isospin doublets $Q_L \equiv (u_L, d_L)^T$ and $L \equiv (\nu_L, e_L)^T$. Right-chiral fields, $\Psi_R \equiv \frac{1}{2}(1 + \gamma_5)\Psi$, are singlets under $SU(2)_L$. Eventually, this will turn out to provide a proper foundation for the experimental evidence that the weak interaction is parity-violating.

The fermion part of the SM Lagrangian is

$$\mathcal{L}_{\text{fermion}} = \sum_{\Psi} \bar{\Psi} i \gamma^\mu D_\mu \Psi, \quad (2.13)$$

where $\Psi = Q_L, u_R, d_R, L, e_R, \nu_R$ ($\times 3$ generations). The covariant derivative, as similarly seen in Eq. (2.2) for QCD, is

$$D_\mu = \partial_\mu - ig_s T^a G_\mu^a - ig \frac{\tau^i}{2} W_\mu^i - ig' Y B_\mu. \quad (2.14)$$

W_μ^i (with $i = 1, 2, 3$) and B_μ are the weak-isospin and hypercharge fields. These fields correspond to the generators of $SU(2)_L \times U(1)_Y$: For the fundamental representation of $SU(2)_L$, τ^i are mapped onto the Pauli matrices, whereas for the trivial representation of $SU(2)_L$, they are mapped onto 0. Thus W^i couple to left-chiral fields only.

The generator of $U(1)_Y$ is the hypercharge operator $Y \equiv Q_{\text{em}} - \tau_3$, where Q_{em} is the electromagnetic charge and τ_3 is the third component of the weak isospin. g and g' are the dimensionless gauge coupling constants.

The gauge term

$$\mathcal{L}_{\text{gauge}} = -\frac{1}{4}G^{a\mu\nu}G_{\mu\nu}^a - \frac{1}{4}W^{i\mu\nu}W_{\mu\nu}^i - \frac{1}{4}B^{\mu\nu}B_{\mu\nu} \quad (2.15)$$

contains, as likewise seen in QCD, trilinear and quadrilinear self-couplings of the gauge bosons. They descend from the non-vanishing commutation relations of the $SU(2)_L$ generators.

Generic mass terms for the electroweak vector bosons V , which are of the form $m^2V_\mu V^\mu$, are not gauge invariant and thus cannot be used to equip the gauge bosons with masses. The Higgs mechanism solves this problem in a consistent way. A complex scalar field ϕ in the fundamental representation of $SU(2)_L$ is introduced. Its properties under gauge transformations are indicated in Tab. 2.1. The scalar enters the Lagrangian with a potential that is constructed to imply a non-vanishing vacuum expectation value, which conveniently is chosen to be $\langle\phi\rangle = (0, v/\sqrt{2})^T$. In this way, the $SU(2)_L \times U(1)_Y$ symmetry is broken spontaneously, where a residual $U(1)_{\text{em}}$ symmetry is retained.

It turns out that the spontaneous symmetry breaking reveals mass terms for two complex and one real linear combination of the W^i and B fields. These massive bosons correspond to the physical W^+ , W^- and Z^0 bosons. A further linear combination, which corresponds to the unbroken $U(1)_{\text{em}}$ symmetry, remains massless. It is identified as the photon.

The Higgs field also is also responsible for the generation of fermion masses. The generic way to introduce fermion masses, *i.e.* via explicit mass terms $-m\bar{\Psi}\Psi$, as done in \mathcal{L}_{QCD} in Eq. (2.1), cannot be used here. In general, they are not invariant under both weak isospin and hypercharge transformations. However, it is possible to couple the fermion and the Higgs field through Yukawa interactions, $-y_e(\bar{L}_R\phi + h.c.)$. Terms of this form can be considered since they preserve gauge symmetry. y_e is a dimensionless coupling constant. After electroweak symmetry breaking, mass terms for the fermions, which are electrons in this case, emerge,

$$-y_e \underbrace{\frac{v}{\sqrt{2}}}_{\equiv m_e} \bar{e}_L e_R + h.c. = -m_e \bar{e}e.$$

3 Event generation with Herwig++

The core of this work is the implementation of a colour reconnection model in the general-purpose Monte Carlo event generator **Herwig++** [1]. An elementary knowledge of the functioning of this program is thus crucial for the comprehension of this thesis. For that reason, the basics of event generation with **Herwig++** are outlined in this chapter.

3.1 Outline

Herwig++ is a program for the simulation of lepton-lepton, lepton-hadron and hadron-hadron collisions at high energies. It handles all parts of this simulation, ranging from the hard process, based on perturbation theory, and the subsequent simulation of QCD radiation, to the formation of the physically observable hadronic final state. This includes the decay of unstable particles.

3.2 Hard process

This stage of the event generation handles the interaction of fundamental incoming particles at high energies, where perturbation theory is valid. In hadron-hadron collisions the flavour of the colliding partons and their momenta are not determined by the experimental setup. These quantum numbers have to be sampled according to parton distribution functions, first. The user, however, chooses which types of processes to take into account. Multiple types of hard processes are generated with the correct fraction according to their cross sections.

Regarding the technical side, only a limited selection of parton-level matrix elements is implemented in **Herwig++**. However, the program is capable of processing events generated by external matrix element generators, e.g. **MadEvent/MadGraph** [14] or **VBFNLO** [15]. This is possible due to the *Les Houches Accord* [16, 17], which specifies a standard format for the exchange of event data between matrix element generators and general-purpose event generators like **Herwig++**, **Pythia8** [18] or **SHERPA** [19].

3.3 Parton shower

One of the integral parts of `Herwig++` is the simulation of hadronic final states, beginning with the outgoing coloured particles from the elementary hard process. The first step to this goal is done by the generation of a parton shower. It evolves partonic states from the hard scale of the subprocess down to hadronic scales, emitting secondary partons.

The parton shower simulation in `Herwig++` is managed by the coherent branching algorithm (*cf.* Sec. 2.3.3) from Ref. [20], which generalizes the one used in `HERWIG` [12]. The angular-ordering property, enabling soft gluon coherence, is preserved. On top, the new algorithm provides invariance under boosts along the jet axis, among other improvements.

The evolution scale t from Eqs. (2.10) and (2.12) is replaced by another variable \tilde{q} , which from now on will be referred to as *the* evolution scale of the parton shower¹. By the choice of \tilde{q} , angular ordering is implemented automatically [1] because $\tilde{q} \mapsto \vartheta(\tilde{q})$ is monotonically increasing.

3.3.1 Initial showering conditions

The initial conditions for the forward and backward showering are determined by the colour flow in the hard process [21]. Colour partners are formed from the coloured particles in the initial and the final state of the hard process. If gluons are involved, this choice is not unique and hence performed on a random basis. The initial evolution scale \tilde{q}_h is calculated from the kinematic properties of the colour-connected partons, including their masses and the scale Q of the hard process.

Additionally, arrangements are made (by appropriate choice of basis vectors in momentum space) that the maximum angle for the first branching in the angular ordered parton shower is determined by the direction of the colour-connected parton. From now on all parton showers are treated independently.

3.3.2 Final-state radiation

Any time-like outgoing parton from the hard process initiates an angular ordered branching cascade, as described in Sec. 2.3. For this task the Sudakov form factor $\Delta(\tilde{q}, \tilde{q}_h)$ is utilized, comparable to $\Delta(t, t_0)$ in Eq. (2.12). It yields the probability of no emission during the evolution from \tilde{q}_h to \tilde{q} .

The showering terminates whenever \tilde{q} falls below its minimal value. This is the case if the phase space is not sufficient for further resolvable emissions. The resulting partons are put on mass-shell.

¹ The definition of \tilde{q} , which actually differs for time-like and space-like branching, can be found in Ref. [1].

3.3.3 Initial-state radiation

To simulate initial-state radiation in hadronic collisions, parton showers backward in time are generated, where the space-like virtuality of the branching partons decreases in each step.

It is worth noting that the backward evolution makes use of a Sudakov form factor that explicitly depends on parton distribution functions (PDFs). In this way, the evolution takes account of the correct probability to find particular flavours with the sampled values of the momentum fraction x and the scale \tilde{q} .

The topology of the first branching is $\tilde{i}\tilde{j} \rightarrow i + j$, where i denotes the space-like parton initiating the hard process and $\tilde{i}\tilde{j}$ the space-like mother parton. The emitted parton j has *time-like* virtuality and may initiate angular ordered time-like parton showers in turn, yielding a simulation of initial-state radiation. This procedure is iterated until the scale falls below a cut-off, which is of order 1 GeV.

In many cases the parton shower will terminate at a stage where a valence (anti-)quark has been produced, since their PDFs dominate at high values of x and low scales. If, however, this is not the case, one or two additional branchings are done in order to force the situation that a valence quark is extracted from the hadron [22].

3.3.4 Colour flow

The parton shower re-sums squared amplitudes of collinear emissions and interference terms where a soft gluon is radiated off a colour triplet-antitriplet pair. The colour structure is thus restricted in the resulting Monte Carlo algorithm: The colour flow in the (probabilistic) parton cascade can be represented by the help of unique colour lines, as depicted in Fig. 3.1. This corresponds to the *large N_C limit* [23], where $1/N_C$ contributions in QCD diagrams are neglected. In this limit the colour charge of a gluon is approximated by a colour-anticolour pair.

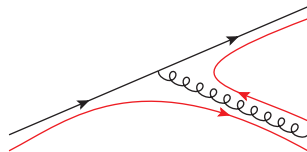


Fig. 3.1 Colour lines in a sample parton splitting process.

3.4 Hadronization

For the hadronization of the parton shower final state, a cluster model [24] is used. In this model, hadronization happens via the formation of colour singlet clusters, which decay into hadrons.

3.4.1 Non-perturbative gluon splitting and cluster formation

The hadronization starts with the final state of the parton shower, consisting of quarks, antiquarks and gluons. In the first step, the gluons are split into quark-antiquark pairs. This happens via a usual two-body decay². Spins are not taken into account, *i.e.* the decay is isotropic. The probabilities for the possible flavours are given by the available phase space in the decay.

After this splitting phase only (di)quarks and anti-(di)quarks are left, which are colour-connected in pairs. A colour singlet cluster is formed from two colour-connected partons each. The momentum of a cluster is given by the sum of the momenta of its constituent partons.

3.4.2 Cluster fission and decay

The next step in the cluster hadronization model is the formation of hadrons from the clusters. This is based on the observation that the cluster mass spectrum is independent of the hard process and its energy. It peaks at low masses, slightly higher than the sum of the masses of the constituent partons. Clusters can thus be regarded as excited hadron resonances and fragment into hadrons.

There is a small fraction of clusters, however, that are too heavy for a direct decay into hadrons. These clusters are first split into lighter clusters using an iterative cluster fission model, which enables appropriate production rates of high- p_{\perp} or heavy particles [25].

For the decay of a cluster ($q_1\bar{q}_2$) into two hadrons, a quark-antiquark pair or a diquark-antidiquark pair ($q\bar{q}$) is extracted from the vacuum (with adjustable probability for the flavour of q). The possible decay products with the flavours ($q_1\bar{q}$) and ($q\bar{q}_2$) are chosen in proportion to the available phase space and the spin degeneracy.

3.5 Underlying event simulation

The simulation of the hard process including the corresponding initial- and final-state radiation is not capable of modelling all hadronic activity that is observed in hadronic high-energy scattering events. Sources of additional (semi-)hard and soft jets need to be included, known as the *underlying event*.

² At the end of the parton shower, all partons are put on their constituent mass-shell. The gluons are given their constituent mass.

3.5.1 Multiple interactions

In `Herwig++` the hard scattering component of the underlying event is accomplished by multiple partonic interactions³ (MPI) [22]. Additional semi-hard QCD $2 \rightarrow 2$ subprocesses with a minimum p_t are generated. This implies further hadronic activity via initial- and final-state radiation.

The final state parton shower is handled in the same way as in the case of the hard subprocess. The initial state showering, however, uses modified parton distribution functions that prevent the shower to terminate in a valence (anti-)quark. If necessary, an additional backward evolution step is done in order to force the shower to end up in a gluon. This has technical reasons: A valence quark is already extracted from the hadron during the generation of the hard subprocess. The two remaining valence quarks form the hadron remnant. A procedure that can be iterated for every additional subprocess is the extraction of a gluon from the beam remnant.

Fig. 3.2 shows the extraction of a valence quark for the hard process and the subsequent extraction of two gluons, ‘initiating’ semi-hard subprocesses. The sketch points out that the subprocesses are colour connected⁴, both among themselves and to the hadron remnant. In the end, clusters of partons stemming from different subprocesses are produced. Sec. 7.2 contains an investigation of the role of *colour reconnection* – a concept introduced in the next chapter – in the case of multiple interactions.

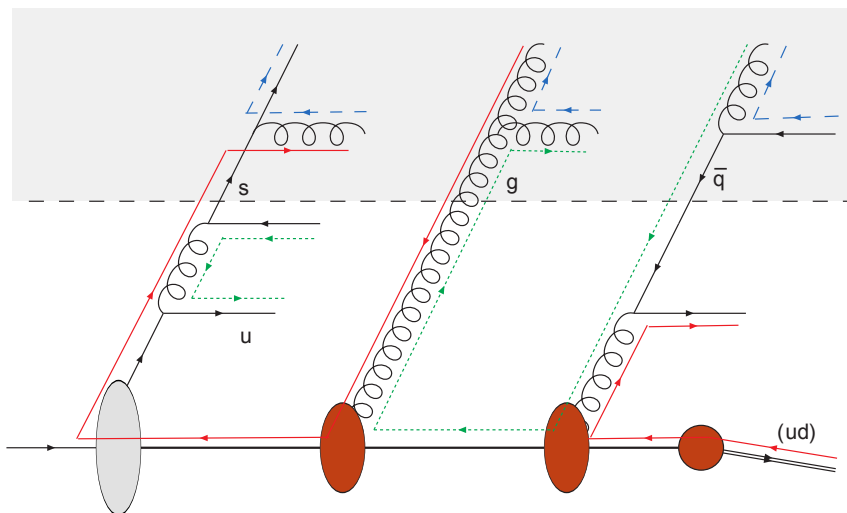


Fig. 3.2 Sketch of the colour connections in the case of additional semi-hard scatterings. The shower at the left belongs to the hard subprocess. It is forced to terminate in a valence quark, which is extracted from the hadron. For every additional subprocess a gluon is extracted from the remnant, inducing colour connections between the subprocesses. Taken from Ref. [22].

³ There is also clear experimental evidence for the existence of multi-parton scattering, e.g. in $\gamma + 3j$ events at CDF [26].

⁴ The MPI model provides the parameter `colourDisrupt`, which gives the probability for an additional subprocess to be colour disconnected from the other subprocesses.

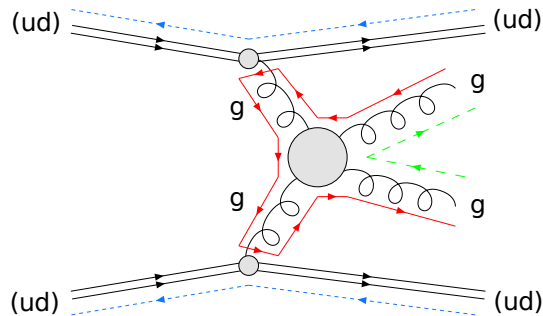


Fig. 3.3 Scattering of soft gluons. Taken from Ref. [1].

3.5.2 Soft interactions

So far the semi-hard part of the underlying event was described. But there are hadronic scatters where no hard jets are produced. To describe soft jets in these events and for the soft part of the underlying event in hard scattering events, **Herwig++** uses a model of non-perturbative soft scattering processes [27].

Provided large centre-of-mass energies s and small interaction scales Q^2 , the parton density functions exhibit a proliferation of gluons at small momentum fractions x . For this reason the soft scattering component of the underlying event is modelled as elastic collisions between soft gluons [1]. The soft gluons are radiated off the valence diquark (or anti-diquark, respectively), which is extracted from the hadron remnant. Fig. 3.3 sketches a typical soft scattering process. The scattering is implemented as a colour singlet exchange, so the colour states of the (anti-)diquarks remain unchanged.

4 Colour reconnection

The best example for the motivation of the *colour reconnection effect* is the process

$$e^+e^- \rightarrow W^+W^- \rightarrow (q_1\bar{q}_2)(q_3\bar{q}_4). \quad (4.1)$$

Two real W bosons are produced, both of which decay hadronically, *i.e.* into a $q\bar{q}$ pair. At this stage there are two massive colour dipoles, $(q_1\bar{q}_2)$ and $(q_3\bar{q}_4)$.

Present parton shower Monte Carlo algorithms, as the one implemented in `Herwig++`, keep the shower generation from both colour singlets completely separate. The subsequent hadron production happens at low, hadronic energy scales where non-perturbative effects dominate. The current chapter covers the study of possible *Crosstalk* between the two initially separate hadronic systems during the entire hadronization process.

4.1 Kinematics

It is worth noting that crucial parts of the kinematics in process (4.1) at the LEP2 experiment are fixed with the experimental setup. The two real W bosons leave the interaction point back-to-back in the laboratory frame. Hence the absolute value of the momentum and the energy of the W bosons are well known. This fact will help in the task of assigning pairs of jets to single W bosons in later analyses of 4-jet events.

The W mass, 80.4 GeV, is not small compared to LEP2 energies, $\sqrt{s} \simeq 189 - 209$ GeV. The transverse momentum p_\perp of a jet, with respect to the direction of motion of the W , can thus be notably high, depending on the decay angle in the rest frame of the W . Assuming $\sqrt{s} = 189$ GeV, the angle in the laboratory frame between a quark-antiquark pair is smaller than about 117° .

4.2 Overlap in spacetime and soft gluon exchange

Process (4.1) produces two $SU(3)_C$ singlets, $(q_1\bar{q}_2)$ and $(q_3\bar{q}_4)$, which shower and fragment subsequently. Because of the small mean lifetime of the W ($\sim 3 \cdot 10^{-25}$ s), the separation of the decay vertices of the two W 's at LEP2 energies is typically $\lesssim 0.1$ fm, which is small compared to the characteristic strong scale of ~ 1 fm. Hence we find that the two hadronization regions are probable to *overlap in spacetime*. An interference between the two hadronic systems via *exchange of gluons* cannot be excluded [28].

4.3 Perturbative colour reconnection

The possibility of *perturbative* colour reconnection and its consequences were first considered in Ref. [29]. The goal of this section is to outline why colour reconnection is strongly suppressed in the perturbative phase of hadronic W pair decays.

In order to obtain a colour rearrangement at matrix element level, one needs at least two gluons to be emitted. The interference term with the Born graph matrix element turns out to be suppressed by a factor $1/N_C^2$ compared to the leading (non-reconnection) $\mathcal{O}(\alpha_S^2)$ contributions.

Additionally, the W bosons live long enough to suppress hard gluon exchange. As seen above, the spacetime separation of the decay vertices is $\mathcal{O}(1/\Gamma_W)$, which has been found to be small compared to hadronic distances. However, this is actually large compared to the length scales for hard gluon emission, $\mathcal{O}(1/M_W)$ in this process.

Taking into account these approximations, the ratio of events with perturbative reconnection can be estimated as [28, 30]

$$\frac{\Delta\sigma^{\text{reco}}}{\sigma} \lesssim \frac{(C_F \alpha_S)^2}{N_C^2} \frac{\Gamma_W}{M_W} \ll 10^{-3}.$$

Colour reconnection at the perturbative level can thus be regarded as negligible.

4.4 Non-perturbative colour reconnection

Since perturbation theory breaks down in the low-energy region, we have to rely on Monte Carlo simulations of the hadronization phase. Thus the effect of *non-perturbative* colour reconnection cannot be estimated as simply as in the perturbative case. An approach to model non-perturbative colour reconnection is to allow soft gluon exchange during the non-perturbative hadronization phase.

In Sec. 3.4 we saw that Herwig++'s hadronization model combines quarks with their colour partners to colourless clusters, which subsequently are utilized to generate hadrons. The exchange of soft gluons during this hadronization phase can be installed by *reconnecting* the colour lines before the cluster creation. This results in the possible clustering of partons that are natively not colour-connected.

This parton re-clustering can be thought of in a simple way: A quark that is about to hadronize together with its colour-connected antiquark could prefer to choose another antiquark that is closer in spacetime. The probability p_{reco} for forming a colour singlet with the new partner is expected to be 1/9: A factor 1/3 is the probability that the antiquark has the matching anticolour charge. Another factor of 1/3 stems from the fact that only one out of three same-colour combinations is actually a colour singlet [30]. Herwig++ de facto operates in the $N_C \rightarrow \infty$ limit. By allowing differently coloured partons to form colour singlet clusters with non-vanishing probability, the limit of large number of colours is explicitly relaxed.

A model that assembles the depicted re-clustering procedure has been considered by Webber in Ref. [30], and is implemented in HERWIG [2]. The re-implementation of this model in the event generator Herwig++ is the central focus of this work.

Colour reconnection has been illustrated to be a *local* phenomenon, as in particular revealed by the reflection about the spacetime-overlap of colour-separated parton shower products. Webber’s colour reconnection model relies on the spacetime structure of the event for the task to model the exchange of gluons in the non-perturbative hadronization phase. This motivates the need for a spacetime picture of the event generation. Because Herwig++ lacks a model producing this information at parton level, another essential topic of this work is the implementation of a spacetime model in this program. Its depiction can also be found in Chapter 5.

4.5 Sensitive observables

4.5.1 Particle flow at LEP2

The production of particles in hadronic W pair events is expected to be affected by colour reconnection during the fragmentation phase [31]. Measurements of charged particles’ multiplicities and their angular distribution with respect to the four jet axes can be used to test colour reconnection models. This has been done by the LEP Collaborations [32–35]. The study of this observable enables the possibility to exclude extreme colour reconnection scenarios. In this way the uncertainty in the measurement of the W mass can be reduced.

4.5.2 Underlying event at the Tevatron

So far we only considered colour reconnection in hadronic W^+W^- decays at LEP2. But colour rearrangements are not restricted to this kind of events: Other examples are $pp/p\bar{p} \rightarrow W^+W^-$, $e^+e^- \rightarrow Z^0Z^0$, $e^+e^- \rightarrow Z^0H^0$ and the like [28].

Further observables that probably require non-trivial colour reconnection effects to be present are related to the *underlying event* in hadronic collisions [36]. From the experimental point of view, the underlying event is defined as every activity in a hadron collision except the two outgoing hard scattered jets. It consists of the beam remnants plus initial and final state radiation (e.g. [37, 38]).

Some observables sensitive to the underlying event simulation and thus probably also for colour reconnection are:

- The mean number of charged particles $\langle N_{\text{ch}} \rangle$ in the ‘transverse’ region¹ versus the transverse momentum of the hardest jet p_{\perp}^{lead} .
- The summed transverse momentum p_{\perp}^{sum} in the ‘transverse’ region versus p_{\perp}^{lead} .

- The average transverse momentum for a given number of charged particles, $\langle p_{\perp} \rangle (N_{\text{ch}})$.

These observables have been or are currently measured at the Tevatron [38–40]. Their simulation, however, turns out to be difficult. There are indications that CDF data favour the presence of a colour reconnection effect to some extent [41].

¹ The ‘toward’, ‘away’ and ‘transverse’ regions in η - φ -space are defined by jet directions. The definition can be found in Ch. 7.

5 Implementation in Herwig++

This chapter gives a description of the implementation of a colour reconnection model in Herwig++. This model is based – as we will see below – on the spacetime structure of the event.

5.1 Spacetime model

In order to receive a spacetime structure for events in Herwig++, an algorithm has been adapted that unifies different simple thoughts in one model. The goal was to generate spacetime points for the production and decay vertices of all partons that are produced during the event generation. Furthermore, a model was required that is able to handle *hadronic* collisions in a reasonable manner, in addition to the (simpler) leptonic case.

5.1.1 Distribution of scattering centres

In the case of hadron collisions, we have to take into account that, in general, there are multiple partonic interactions during one collision. In a realistic model, the scattering centres of these interactions do not coincide in one point. On the contrary, they must be modelled to be distributed over the entire spatial extent of the colliding hadrons.

In a first step the problem to generate the spacetime point (t^*, x^*, y^*, z^*) is reduced from four to effectively two dimensions, using the following simplifications:

$z^* \equiv 0$ Scattering centres are generated in the x - y plane only. In beam direction (= z direction), protons at the LHC are notably Lorentz contracted. In the laboratory frame, a proton's size in z direction amounts only approximately 0.013 % of the value in its rest frame (a centre-of-mass energy of 7 TeV provided). Hence the z length scale is negligibly small compared to the ones in x and y direction.

$t^* \equiv 0$ All interactions happen simultaneously.

Thus we need a spatial parton density in the x - y plane. This model assumes that the spatial density of the electric charge in the hadron is a good approximation for the spatial parton density. It can be derived from the electromagnetic form factor.

The following probability density for the scattering centres' distances from the origin in the x - y plane is used:

$$A_\mu(b) = \frac{\mu^2}{96\pi}(\mu b)^3 K_3(\mu b). \quad (5.1)$$

It satisfies

$$\int d^2\mathbf{b} A_\mu(b) = 1,$$

where K_3 is the modified Bessel function of the third kind.

The model parameter μ in Eq. (5.1), that has the dimension of an inverse length, can be referred to as the inverse hadron radius. In elastic e - p scattering a value of $\mu^2 = 0.71 \text{ GeV}^2$ yields the best description of the data [42], which therefore is the default value for μ^2 in the present model. However, the possibility to change μ^2 is retained since the spatial density of the electric charge is not guaranteed to coincide with the spatial density of the colour charge.

In Herwig++'s multi-parton interaction model (introduced in Section 3.5.1) the same probability density is used as an expression for the spatial overlap of colliding hadrons as a function of the impact parameter b . It is utilized to generate the number of additional partonic scatterings [27, 43].

Details on how to sample the remaining two components $\mathbf{b} = (x^*, y^*)$ according to Eq. (5.1) can be found in Appendix A. The creation points of the (anti-)proton remnants are set to the spacetime point $(0, 0, 0, 0)$. A remnant is what remains from the hadron after the extraction of the partons that initiate hard processes.

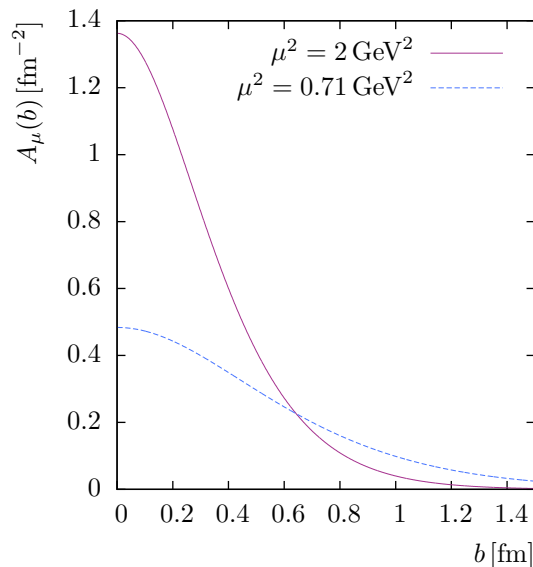


Fig. 5.1 $A_\mu(b)$ for two values of μ^2

5.1.2 Lifelength generation

At this stage each partonic subprocess has a spacetime point assigned. This spacetime information is required to propagate throughout the remainder of the event generation.

For this purpose a model has been adopted that is already used in the event generator HERWIG [25].

Mean lifetime

For the mean lifetime τ of a virtual parton we use

$$\tau(q^2) = \frac{\hbar}{\sqrt{4(\sqrt{q^2} - m)^2 + \frac{\Gamma^2 q^2}{m^2}}}. \quad (5.2)$$

where m denotes the constituent mass of the parton¹. This expression has its roots in Heisenberg's uncertainty principle, its derivation is presented in Appendix B.

Eq. (5.2) interpolates between $\tau_0 = \hbar/\Gamma$ for an unstable particle on mass-shell and

$$\tau_{\text{no width}}(q^2) = \frac{\hbar/2}{|\sqrt{q^2} - m|}$$

for a particle far off mass-shell that has no natural width, as Fig. 5.2 may illustrate. We use Eq. (5.2) for particles with time-like momenta, $q^2 > 0$, whereas for $q^2 < 0$ we set $\tau \equiv 0$.

We introduce a lower limit on the natural width, $\Gamma_{\min} = v_{\min}/m$. This limit prevents path lengths of partons with small widths from exceeding typical hadronization lengths, which is of particular importance for partons with low virtuality at the end of the parton shower. It can be regarded as an effective minimal virtuality bound, too.

While in HERWIG this bound applies to light quarks and gluons only, we use it for every parton. This includes also diquarks, for whom Eq. (5.2) yields infinite lifetimes in the case of no virtuality because the natural width vanishes.

If there are gluons after the parton shower has ended, they undergo a forced splitting into quark-antiquark pairs (see Sec. 3.4.1 on Herwig++'s cluster hadronization model). For these gluons we set $\tau = \hbar m/v_{\min}$.

Sampling

Given the mean lifetime, the proper lifetime t^* of a parton (in its rest frame) is sampled according to an exponential decay law. The probability that the parton is decayed at the time t is

$$\mathcal{P}(t^*) = 1 - \exp\left(\frac{-t}{\tau}\right). \quad (5.3)$$

This implies

$$t^* = -\tau \ln \mathcal{R} \quad (5.4)$$

as a prescription to yield a proper lifetime, sampled according to the distribution (5.3). \mathcal{R} is a random number between 0 and 1.

¹ E.g. $m_u = 0.325$ GeV and $m_g = 0.95$ GeV are used in Herwig++ version 2.4.2.

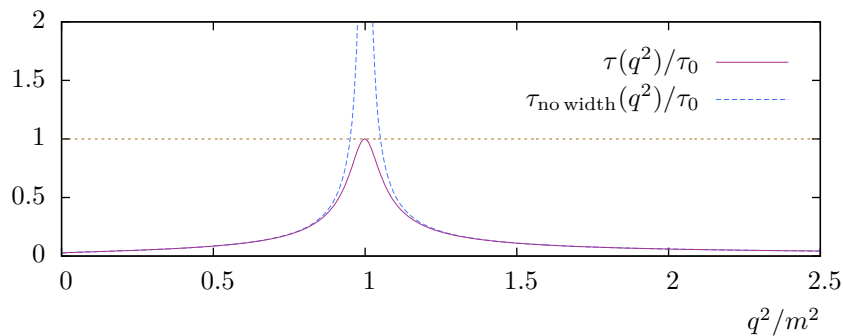


Fig. 5.2 Mean lifetime as a function of the virtuality for the case $\Gamma = 0.05 m$.

Lorentz boost and path length

The lifetime t^* that has been sampled now is the proper time in the particle's rest frame. In order to obtain the decay vertex for a given production vertex in the laboratory frame, we have to perform a Lorentz boost to the laboratory frame at first,

$$t = \gamma t^*$$

with $\gamma = 1/\sqrt{1 - \beta^2}$ and $\beta = |\mathbf{q}|/E$ the velocity. The distance travelled by the particle in the laboratory frame is then

$$d = \beta t,$$

whereas the direction of motion is obviously the momentum direction $\hat{\mathbf{q}}$. Combining all four components yields compactly

$$d^\mu = \frac{t^*}{\sqrt{q^2}} q^\mu.$$

5.1.3 Combining the sub-models

We get the spacetime structure of the event by combining the information collected so far. The rough structure of the algorithm is as follows:

- (a) For every subprocess generate a spacetime point.
- (b) Intermediate particles of the subprocesses (e.g. gauge bosons in the s or t channel) get their production and decay vertices set to the same point.
- (c) Step through the initial-state parton showers backward in time, beginning with the subprocesses. Construct the vertices for these particles until the colliding particles are reached. This part is trivial in the case of colliding leptons for there is no initial state parton shower in this case.
- (d) Set the creation vertex of the (anti-)proton remnants to $(0, 0, 0, 0)$.

- (e) Step through the event forward in time beginning with the colliding particles and construct all vertices that are not set yet. This last step covers *all* final state parton showers, *i.e.* the showers induced by time-like partons produced during the hard subprocesses as well as showers from time-like partons generated during the initial-state shower. Furthermore, the phase where time-like gluons are split is also handled in this step.

5.1.4 Plausibility check

In order to get a rough idea whether this spacetime model does a reasonable job, we are well advised to study the lifetimes and path lengths of the partons in the parton shower. Reflecting that the hadronization happens at typical length scales of $1/\Lambda_{\text{QCD}} \approx 1 \text{ fm}$, we should assert that the model produces travel distances coinciding with this order of magnitude.

As Figs. 5.3(a) and 5.3(b) reveal, the travel distance distribution depends strongly on v_{min} , the minimal virtuality bound introduced above. By raising its value, one can suppress the mean lifetime and thus manage to move the lifetime distribution to smaller values of τ (*cf.* Fig. 5.3(c)). The travel distance distribution is influenced analogously. In fact, the bulk of the travel distances is populated below 1 fm. However, there is also a tail representing partons that travel over longer distances.

All these arguments must not be taken too literally. What we get from perturbation theory are scattering amplitudes, that do not provide any spacetime information, at all. Furthermore, this is an attempt to model a quantum mechanical process like a hadronic collision with classical methods. For instance, the quantum numbers momentum and position of the particles produced by the Monte Carlo event generator are known exactly. That the model complies with the QCD scale is thus an admittedly rather naive argument, which is more or less only an indication that we can allow a colour reconnection model to be based on this implementation.

The default value of the model parameter v_{min} is chosen to be 0.5 GeV^2 , which is used throughout the analyses in Chapters 6 and 7. Needless to say, before using this model in future analyses, this parameter must be retuned, together with the other **Herwig++** parameters. However, an overall retuning of the parameters with the (spacetime based) colour reconnection model enabled (see below) could not be covered within the scope of this work.

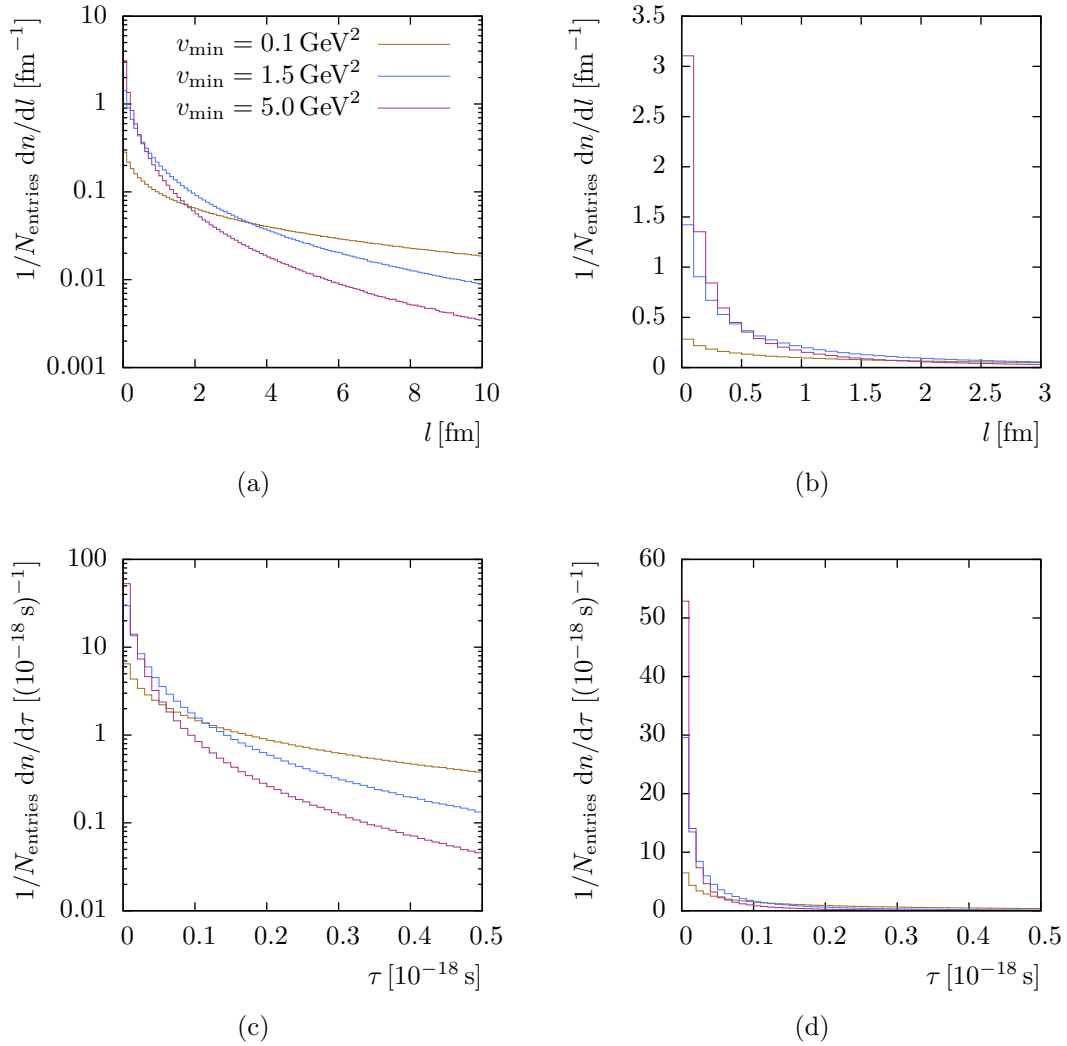


Fig. 5.3 Travel distance and lifetime distributions (in the laboratory frame) for partons in the final state parton shower. Parton showers initiated by two outgoing partons (gluons or quarks) from $2 \rightarrow 2$ QCD subprocesses at the LHC were studied here. Only partons with lifetimes > 0 (or travel distances > 0 , respectively) were allowed to contribute to the histograms.

All distributions are normalized to the entire number of entries in the respective histogram. This includes also those entries that exceed the upper visible histogram limits. Figures (a) and (b) show the same distributions, scaled differently, likewise (c) and (d).

5.2 Colour reconnection model

5.2.1 Introduction

The colour reconnection model that has been implemented is in its ideas identical to the one implemented HERWIG. Ref. [2] depicts the original implementation by Webber, who presents the physical ideas appropriately in Ref. [30].

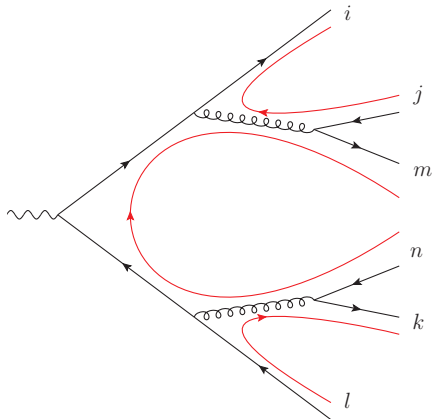


Fig. 5.4 Sketch of a sample parton shower. In the final state each quark is colour-connected to an antiquark, which is represented by red colour lines. These allocations are unambiguously determined by the flavour structure of the parton shower.

On the basis of Fig. 5.4, the colour reconnection algorithm is easy to understand. A sketch of a sample parton shower is shown, e.g. initiated by a hadronically decaying electroweak boson. The quark-antiquark pairs in the final state are colour-connected. As discussed in Sec. 3.3.4, the routes of the colour lines are uniquely determined by the flavour structure within the parton shower.

The quark-antiquark pairs² – in this example denoted by (ij) , (mn) , and (kl) – are colour singlets. Herwig++’s hadronization model treats them as *clusters*, from which hadrons are generated finally.

Soft gluon exchange during this phase, as considered in Sec. 4.4, implies, in the limit of no momentum transfer: The colour lines at the end of the parton shower are allowed to be reconnected. Of course, such a gluon exchange must not be understood literally in the sense of closed loops in Feynman diagrams. It is questionable anyway whether partonic degrees of freedom can be considered as suitable in the realm of non-perturbative physics. From this point of view, this approach must be regarded as a *model* that tries to enhance the original, quasi-colour-agnostic parton shower model.

5.2.2 Algorithm

For a cluster (ij) consisting of the *coloured* constituent q_i and the *anticoloured* constituent \bar{q}_j (i and j for short) we define d_{ij} to be the space time distance between the

² In general, one would refer to colour-anticolour pairs, taking into account that also anti-diquarks (diquarks) can be in the fundamental (anti-fundamental) representation of $SU(3)_C$.

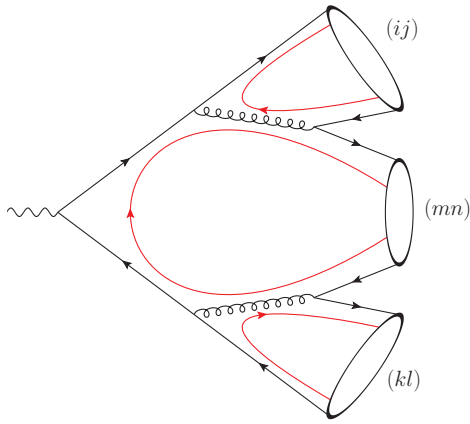


Fig. 5.5 Clustering without colour reconnection

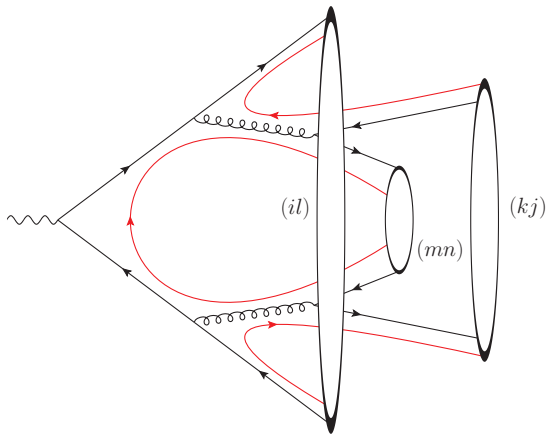


Fig. 5.6 A possible alternative cluster topology: Other pairs of partons, (il) and (kj) , are combined to clusters.

constituents' production points v_i and v_j ,

$$d_{ij}^\mu = v_i^\mu - v_j^\mu.$$

The colour reconnection procedure starts with the original clusters, consisting of the pristine colour-connected parton pairs. The following steps are done for each cluster (ij) where the order of the clusters is randomized:

1. Find the cluster (kl) that is *closest* in spacetime: This is the cluster containing the anticoloured parton l which has a minimal distance $|d_{il}|$.
The selection algorithm assures that neither of the potential new clusters, (il) and (kj) , is a colour octet (see Sec. 5.2.3)
2. Check if a reconnection with this cluster³ lowers the sum of the squared Lorentz invariant spacetime distances between the clusters' components,

$$|d_{il}^2| + |d_{kj}^2| < |d_{ij}^2| + |d_{kl}^2|. \quad (5.5)$$

If this condition holds, accept the reconnection with probability p_{reco} (default value⁴ is 1/9): The clusters (ij) and (kl) are replaced by (il) and (kj) .

³ There are exactly two cluster combinations for the partons i, j, k and l : The pristine clusters (ij) and (kl) or the reconnected clusters (il) and (kj) .

5.2.3 Colour octet veto

In step 1 of the colour reconnection algorithm from above, we explicitly disallow colour octet clusters to be built. For example the rearrangement $(ij), (mn) \rightarrow (in), (mj)$ (with the names as in Fig. 5.4) is prohibited because m and j descend from the same gluon and thus formally embody a colour octet.

Note, that the reason for this veto is not entirely group theoretical in nature. Actually, the suppression of colour octet clusters is also taken into account by the additional factor $1/3$ in p_{reco} (cf. Sec. 4.4).

The main difficulty with the (mj) cluster is the vanishing size d_{mj} . This would result in a model where the clustering of products of non-perturbative gluon splittings (see Sec. 3.4.1) is unreasonably highly preferred. On top of that, the mass of colour octet clusters is exactly the gluon constituent mass (950 MeV). A narrow peak in the cluster mass distribution would be the consequence, as can be seen in Fig. 5.8.

It is important to emphasize that this veto only applies to colour octet states generated at the very end of the parton shower or during a forced gluon splitting. Clustering candidates with a colour combination that somewhere earlier in the parton shower built up a colour octet state (as the colour of a gluon) are allowed.

5.2.4 Cluster mass distribution

The mass spectrum of primary clusters⁵ generated by Herwig++'s parton shower in e^+e^- collisions has been shown to be *independent* of the hard scale Q^2 of the process [44]. The typical cluster mass is of $\mathcal{O}(Q_0)$, where Q_0 is the infrared cut-off of the parton shower [43]. *Primary* clusters are clusters that are directly generated from the final state of the parton shower or a subsequent gluon splitting, respectively. This definition excludes clusters that are generated during the fission of heavy clusters into lighter clusters (see Sec. 3.4).

It is interesting to trace possible changes in this characteristic mass spectrum that come with the re-clustering during the colour reconnection. In Fig. 5.7 the mass of light clusters, *i.e.* clusters consisting of light partons only (u , d and s), is shown. The minimal mass of a cluster is $2m_{\text{light}} \simeq 0.6$ GeV, where m_{light} is the constituent mass a light quark. The original spectrum shows that the cluster mass is preferably populated at small values, right above the threshold. The colour reconnection model reduces the cluster mass on average.

Fig. 5.8 demonstrates what happens if the products of non-perturbative gluon splittings were allowed to be clustered. A narrow peak at the constituent mass of the gluon emerges. This could influence the flavour spectrum of the generated hadrons. Additionally, the fixed available phase space for the hadrons could disturb the transverse momenta of the hadrons with respect to the cluster direction. These are surely effects

⁴ A simple argumentation, based on the SU(3) group structure, gives rise to expect $p_{\text{reco}} \approx \frac{1}{9}$ (cf. Sec. 4.4).

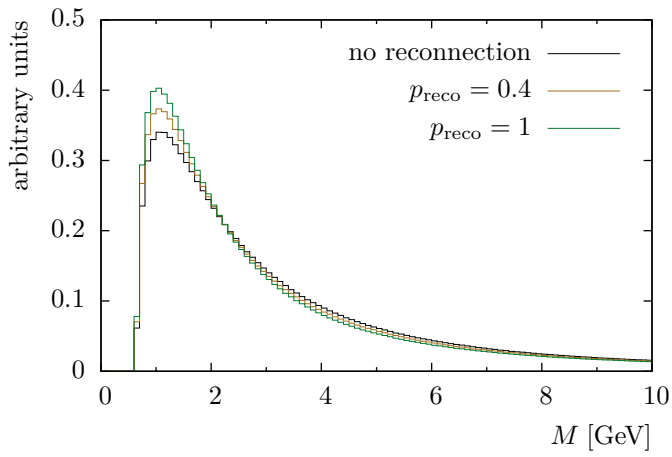


Fig. 5.7 Mass distribution of primary light clusters in e^+e^- collisions.

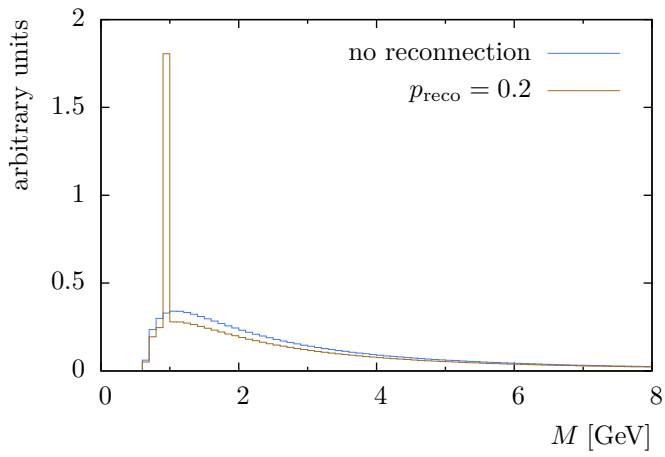


Fig. 5.8 Mass distribution of primary light clusters in e^+e^- collisions if colour octet clusters were allowed.

that should be avoided. Thus the formation of colour octet clusters is forbidden in the reconnection algorithm in Sec. 5.2.2.

6 Particle flow in WW events

The present chapter contains an analysis of the charged particle flow in hadronic WW events at LEP2, which is an observable that promises to be sensitive to colour reconnection. The main purpose of this analysis is to examine the impact of non-perturbative colour reconnection on LEP data. Before the new model can be applied in the context of more recent physics at hadron colliders, it should produce reasonable results in well understood LEP analyses.

Originally proposed in Ref. [45], the DELPHI Collaboration performed particle flow studies in Ref. [32]. The analysis in this chapter is oriented towards this work: All instructions for the proceeding in this analysis and the experimental data are taken from this reference.

6.1 Analysis details

This section covers details of the realization of the particle flow analysis. Since the definition of the inter-jet regions in $WW \rightarrow 4j$ events is non-trivial and actually differs in analyses by other LEP Collaborations [33–35], a detailed recapitulation of the procedure may be helpful.

The analysis itself is done in `Herwig++`, using the provided `ThePEG::AnalysisHandler` base class. After the generation of an event in `Herwig++`, it is presented to the `AnalysisHandler` implementation. At this stage cuts in the final state can be applied (see below) which decide if the event contributes to the analysis. The `AnalysisHandler` has not only the possibility to analyse the event's final state, but it can access all steps of the event generation.

6.1.1 Hard process

The further analysis will show that efficiency to select $WW \rightarrow 4j$ events by means of experimentally accessible information is not high. Hence it is not reasonable to neglect the background and to generate signal events (hadronically decaying W pairs) only.

The preferred way is thus to produce signal events together with the most important background events and to apply nearly the same cuts and event selection criteria as done in the experiment. The price we pay is an extremely sparse efficiency of $\sim 2\%$ surviving events, as we will see below.

The generated hard processes are

- (a) $e^+e^- \rightarrow W^+W^- \rightarrow (q\bar{q})(q\bar{q})$,
- (b) $e^+e^- \rightarrow W^+W^- \rightarrow (q\bar{q})(l\nu)$,
- (c) $e^+e^- \rightarrow Z^0Z^0$,
- (d) $e^+e^- \rightarrow \gamma^*/Z^0 \rightarrow q\bar{q}$,

where the reader may recognize the first one as the signal process. Needless to say, **Herwig++** produces the hard processes in the correct frequencies according to the respective cross sections.

Actually, the fully leptonic decay of W pairs, $e^+e^- \rightarrow W^+W^- \rightarrow (l\nu)(l\nu)$, is also generated. This is because of technical reasons: Disabling the leptonic decay channel of the W boson at generator level would eliminate semi-leptonic processes of type (b), too. However, these events are discarded from further analysis because they do not pass the event selection criteria below.

6.1.2 Event selection

In order to be able to compare the Monte Carlo (MC) data to DELPHI data, we obviously have to apply the same selection criteria and cuts to the events as has been done with experimental data, summarized in Ref. [32].

Pre-selection

To reduce contributions from $\gamma\gamma$ events to a negligible amount, the DELPHI Collaboration requires

- at least 12 charged particles in total
- and $\sum_{\text{visible particles}} |\mathbf{p}_\perp| > 20\% \cdot \sqrt{s}$,

Tab. 6.1 Ratio (in %) of MC events (mixed sample with all processes, signal, semi-leptonic, leptonic WW decays, ZZ and $q\bar{q}(\gamma)$ events) that **fail** the various selection criteria. The last line contains the ratio of events that are left after the selection procedure. The data are collected with $\sqrt{s} = 189$ GeV and colour reconnection switched off.

	mixed	signal	semi-l.	leptonic	ZZ	$q\bar{q}(\gamma)$
pre-selection	6.1	0.002	4.5	100.0	10.8	5.0
lower bound for \hat{s}	56.3	0.0	0.0	0.0	0.0	66.3
jet constraints	30.0	36.6	82.6	0.0	50.1	25.9
kinematic jet pairing	5.6	41.9	9.4	0.0	24.2	2.4
surviving events	2.0	21.6	3.4	0.0	15.0	0.4

Tab. 6.2 Like Table 6.1, but with $\sqrt{s} = 200$ GeV.

	mixed	signal	semi-l.	leptonic	ZZ	$q\bar{q}(\gamma)$
pre-selection	6.3	0.002	4.5	100.0	10.7	4.9
lower bound for \hat{s}	54.1	0.0	0.0	0.0	0.0	66.0
jet constraints	31.3	37.5	84.8	0.0	50.7	26.3
kinematic jet pairing	6.4	45.0	8.5	0.0	24.5	2.4
surviving events	2.0	17.5	2.2	0.0	14.1	0.4

where \mathbf{p}_\perp is a particle's transverse momentum with respect to the beam axis, and \sqrt{s} is the centre-of-mass energy of the colliding particles.

The second requirement sums over the transverse momentum of all *visible* particles in the DELPHI data. Neutrinos, which occur in leptonic W decays, are not included. Our analysis of Monte Carlo data takes *all* final state particles into account. This could lead to a systematic error, which, however, can be estimated to be small since only $\sim 3\%$ of events with leptonic W decays survive all selection criteria (*cf.* Tabs. 6.1 and 6.2).

Although the MC data sample contains no $\gamma\gamma$ events, this constraint has been adopted in order to assure that the MC events are suppressed and selected in the proper ratio.

Tab. 6.1 indicates that leptonic W pair decays, that have been generated unnecessarily, are completely cut out by these requirements since the number of charged particles in the final state is too small. Furthermore, we see that this constraint does almost never affect signal events.

Radiative return

Process (d) also includes so-called *radiative return* events, where a hard photon is radiated off the colliding e^+e^- pair. In this way, the invariant mass $\sqrt{\hat{s}}$ of the lepton pair after the emission of the hard photon approximately 'returns' to the Z^0 mass, where the $e^+e^- \rightarrow q\bar{q}$ cross section peaks.

In the original analysis by DELPHI, $\sqrt{\hat{s}}$ is estimated as described in Ref. [46]. That method uses the 4-momenta of jets and photons in the final state and estimates also contributions from an eventually undetected photon in the beam line. Our Monte Carlo analysis, however, obtains $\sqrt{\hat{s}}$ directly from the event generator. It is defined as the centre-of-mass energy of the colliding lepton pair after the initial-state radiation has finished.

To suppress major parts of the $e^+e^- \rightarrow q\bar{q}(\gamma)$ background, the effective centre-of-mass energy is required to be sufficiently above the Z mass,

$$\sqrt{\hat{s}} > 110 \text{ GeV}. \quad (6.1)$$

The respective suppression ratios (‘lower bound for \hat{s} ’) in Tab. 6.1 and 6.2 reveal the efficiency of this requirement: About 2/3 of the $q\bar{q}(\gamma)$ events do not pass this filter, whereas signal events are not affected, at all.

Jet constraints

An accepted event is required to have exactly four¹ jets constructed with the Durham jet algorithm [47] with the resolution parameter $y_{\text{cut}} = 0.005$. Additionally, the multiplicity of charged and neutral particles in each jet is required to be larger than three.

This constraint has two important effects: First, it removes the bulk of the background processes with 2- or 3-jet signature or too small multiplicity (confer Tab. 6.1 and 6.2). And the second effect is obvious: It selects only hadronic WW events with 4-jet signature.

6.1.3 Identification of jet pairs

The further analysis happens in four steps: The association of jet pairs with W bosons, the definition of four inter-jet planes spanned by the jet momenta, the projection of the particles onto these planes and the actual analysis of the multiplicity distribution in these planes.

Identification via angle cuts

The identification of jet pairs from the experimental point of view completely happens via the help of kinematic considerations. The situation is not entirely trivial since we look at 4-jet events: In general, these jets are not coplanar. The method followed by DELPHI is to apply cuts in the jet-jet angles, six of whom there are, altogether. This is accomplished in the following steps:

- The two smallest jet-jet angles must satisfy

$$\Phi_{\text{small}} \leq 100^\circ$$

and must not have a common jet. The dijets connected to these angles will finally define the *between-W* regions, cf. Fig. 6.2.

- For two other angles (the ‘large’ angles) the condition

$$100^\circ \leq \Phi_{\text{large}} \leq 140^\circ$$

must hold. They are also not allowed to have a common jet. The *inside-W* regions are defined by the two dijets corresponding to these angles.

¹ For the jet clustering the FastJet package [48] was used, which provides libraries that implement the Durham algorithm.

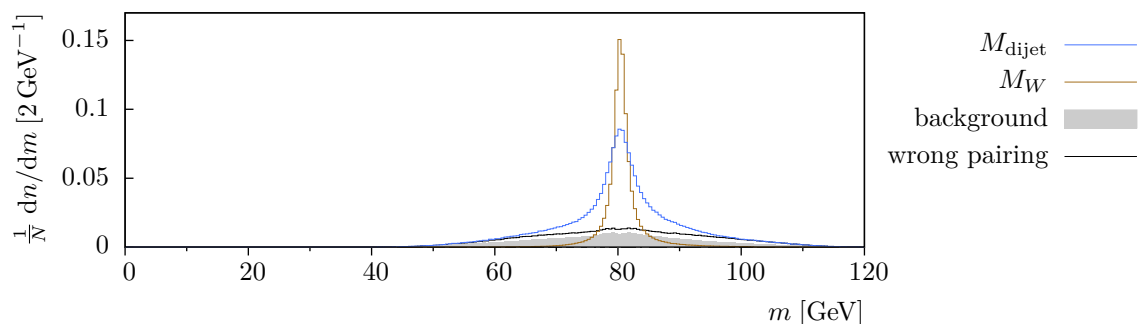


Fig. 6.1 Invariant dijet mass at 189 GeV, compared to the invariant mass of the W bosons. Both the M_{dijet} histogram and the M_W histogram contain two entries per event. These two histograms are normalized to unity, whereas the M_W histogram has been divided by 2 afterwards. The background histogram shows the fraction of dijets originating from the background processes. The histogram labelled by ‘wrong pairing’ contains WW events for which the dijets were formed wrongly, added to the background events.

- If this prescription yields an ambiguous result, *i.e.* if more than one combination of jets fits these constraints, the combination with the highest sum of ‘large’ angles is chosen.

Note that the lower cut in the ‘large’ angles, $\Phi_{\text{large}} \geq 100^\circ$, is chosen to provide a lower limit on the angle between jets originated from the same W boson. In Sec. 4.1 we saw that in this process the angle between the *partons* from a W decay is smaller than $\sim 117^\circ$. In a rough approximation, this applies also to the angle between the respective *jets*.

The selection criteria were designed in order to minimize the situation of one jet from one W boson appearing in the *inside- W* region of the other W boson [32]. For $\sqrt{s} = 189$ GeV only $\sim 34\%$ of the events that passed all previous criteria satisfy these cuts.

Invariant dijet mass

Fig. 6.1 depicts the invariant mass of the paired jets, which peaks at M_W , but which is more spread than the Breit-Wigner distribution of the invariant W mass. There are two obvious reasons for that: First, there are still background events and $WW \rightarrow 4j$ events with wrongly paired jets. The second and more important reason hides in the nature of jets. The jet algorithm clusters particles to jets that do not necessarily have a common history but rather fulfil kinematic criteria. Thus, in general, the invariant dijet mass differs from the invariant mass of the corresponding W , even for correct jet pairing. Applying additional kinematic constraints for the jet momenta can improve the W mass resolution [49].

Cross check: Dijet identification at generator level

Of course, within Herwig++ there is the possibility to trace back the histories of the final state particles. This supplies the possibility to figure out for every particle in the final state whether it descends from the W^+ or the W^- boson.

Note, that without colour reconnection this origin is unique: Consider a hadron in the final state. It is originated from a cluster whose both constituents are colour-connected, *i.e.* cannot descend from different parton showers. Hence the assignment of a hadron to one of the two W bosons is unambiguous. With colour reconnection enabled, however, the situation is more complicated. Partons from different parton showers, *i.e.* showers originated by different W decays, are allowed to be clustered. In this case it is reasonable to identify a cluster's origin as the origin of its most energetic constituent.

In this way a *definition* of a jet's origin is possible: If more than 75% of a jet's energy stems from boson A , it is *assigned* to this boson, likewise for boson B . Note that this energy fraction is chosen arbitrarily.

Now there are three cases:

- (i) Two jets stemming from the W^+ and two from the W^- boson are found. This is interpreted as a successful pairing.
- (ii) There is a jet that cannot be assigned to either of the W bosons. This happens if the energy fraction descending from one boson is in the interval [25%, 75%].
- (iii) The number of jets descending from W^+ differs from the one descending from W^- .

Events satisfying case (ii) or (iii) do not contribute to the calculation of the pairing efficiency in Tab. 6.3. However, they are retained in the further analysis.

With this definition a jet assignment at generator level is successful in $\sim 91\%$ of the analyzed $WW \rightarrow 4j$ events at $\sqrt{s} = 189$ GeV (*cf.* Tab. 6.3). This fraction can probably be enhanced by adapting the energy threshold in the definition above. However, the generator-side jet pairing is only done in order to gain information on the efficiency of the (experimental) jet pairing.

As summarized in Tab. 6.3, the pairing efficiency is roughly 90%.

Tab. 6.3 Ratio of events for which the generator-side pairing algorithm succeeds, and of those events the fraction where the pairing via angle cuts coincides.

\sqrt{s} GeV	jet assignment possible %	pairing efficiency %
189	90.9	84.9
200	91.7	92.6
206	90.5	90.9

6.1.4 Definition of inter-jet regions

The algorithm to find the two jet pairs is described in Sec. 6.1.3. This was done by imposing cuts in four of the six jet-jet angles. The algorithm returns four pairs of jets, each of which spans a plane in 3-dimensional momentum space. These planes (or regions) are labelled as follows:

- **region A** is the region with the greater one of the two ‘large angles’ found by the algorithm in Sec. 6.1.3. ($100^\circ \leq \Phi_A \leq 140^\circ$)
- **region C** is the region with the smaller one of the two ‘large angles’. Note that the two ‘large’ angles, defining the inside- W regions A and C , are not necessarily the two largest inter-jet angles. ($100^\circ \leq \Phi_C \leq 140^\circ$)
- **region B** is the region corresponding to the smallest angle. ($\Phi_B \leq 100^\circ$)
- **region D** is the region with the second smallest angle. ($\Phi_D \leq 100^\circ$)

The jets are enumerated as shown in Fig. 6.2. *E.g.* the jet that borders regions A and B is called *jet 1*, etc.

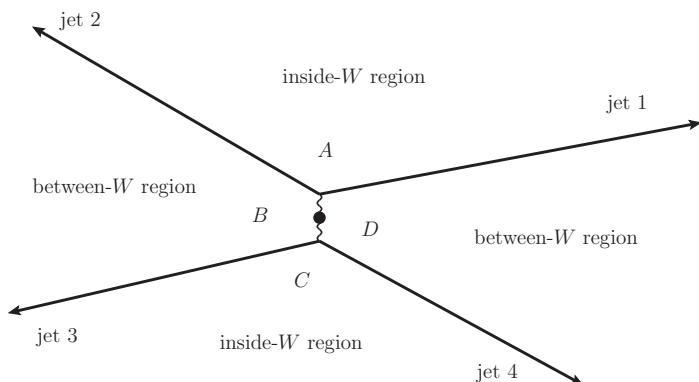


Fig. 6.2 Sketch of the jet topology in a $WW \rightarrow 4j$ event. In general, however, the jets are not coplanar. This 2-dimensional schematic drawing is thus a simplification.

6.1.5 Assignment of particles to inter-jet regions

Any *charged* particle (or its momentum vector, to be precise) is projected onto the four planar regions. The particle is attributed to the region where the projected momentum vector is located between the jets, as shown in Fig. 6.3. If this is ambiguous ($\sim 13\%$ of the particles on average), the region is chosen where p_\perp relative to the plane is minimal. It is also possible, that a particle cannot be projected onto any of the four regions. This is the case for about 8.5% of the particles. Those particles are omitted from further analysis.

We are now ready to study the particle flow in the jet-jet planes as a function of the rescaled angle in the projection plane,

$$\Phi_r = \frac{\varphi}{\Phi_{\text{jet-jet}}}, \quad (6.2)$$

which, by definition, is between 0 and 1 for each particle.

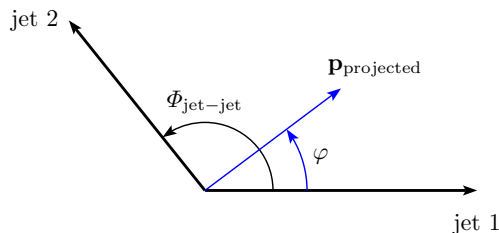


Fig. 6.3 Projection of particles onto planes spanned by jet momenta. The angle φ is always measured from the jet with the smaller index, except in the case of jet 4 and jet 1.

6.2 Expected results

The implemented colour reconnection model allows clusters and thus hadrons to be composed of partons that are originated by different W decays. Hence in events with 4-jet-like signature, where pairs of jets can be assigned to the W bosons, the colour reconnection model is expected to enhance the hadron production preferably in the *between- W* regions, *i.e.* in regions B and D .

Quantitatively, the ratio of the charged particle flow in the *inside- W* regions over the flow in the *between- W* regions is expected to decrease with the rate of colour reconnected clusters.

Further, since the colour reconnection model is based on physically justified considerations (see Ch. 4), it is supposed to improve the Monte Carlo simulation in the sense of gaining a more accurate reproduction of experimental results.

6.3 Particle flow distribution

In Fig. 6.4 the charged particle flow distribution for 189 GeV is shown. All four planar inter-jet regions combined in one plot, *e.g.* region B is plotted in the Φ_r range between 1 and 2. The plot contains experimental data taken from DELPHI's particle flow analysis in Ref. [32]. They are compared to **Herwig++** data using various colour reconnection settings.

The histogram showing **Herwig++** data without colour reconnection reveals that too much hadronic activity between the jets ($\Phi_r \in \{[0.2, 0.8], [1.2, 1.8] \dots\}$) is generated by the parton shower and hadronization models. A possible way to influence this observation is to artificially suppress the evolution scale at which the (final-state) parton shower evolution is started after the hard process. This idea is pursued in Sec. 6.6.1.

Moreover, a slight increase of the particle flow in all inter-jet regions can be observed. In Fig. 6.4 one can barely recognize that the enhancement in the *between- W* regions, B and D , is stronger. The investigation of the flow ratio in the next section provides answers to this question.

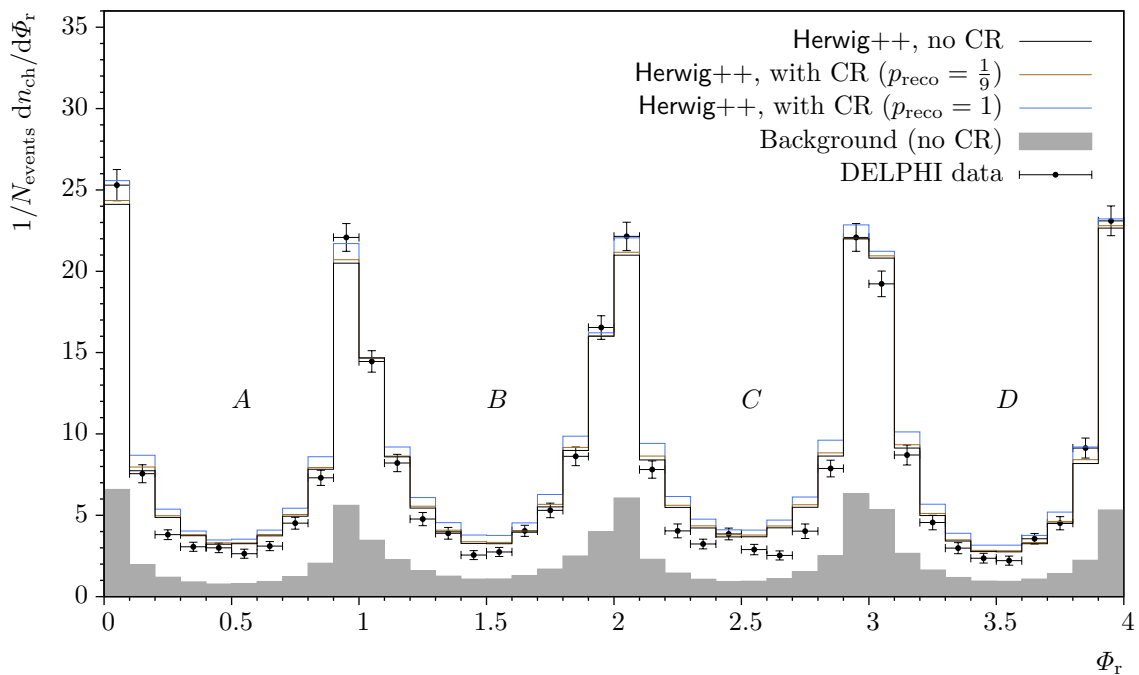


Fig. 6.4 Charged particle flow distribution at 189 GeV. The histograms are normalized to the total number of analyzed events (signal plus background). Thus the integral of each histogram (except the background histogram) is the mean number of analyzed charged particles per analyzed event.

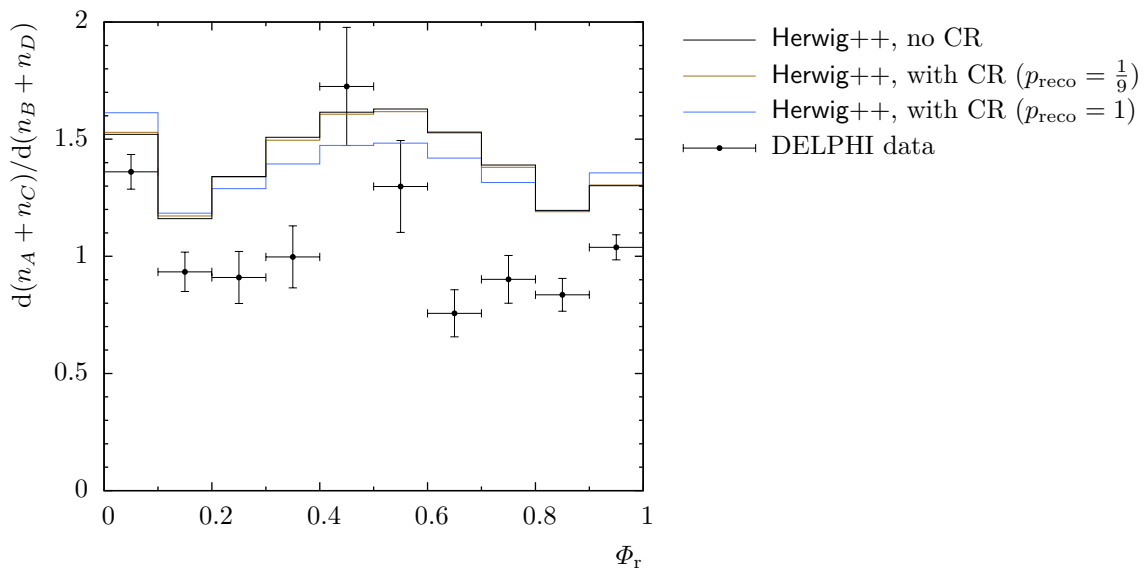


Fig. 6.5 Bin-by-bin ratio of the charged particle flow in *inside-W* over *between-W* regions at 189 GeV. Before calculating the ratio $(n_A + n_C)/(n_B + n_D)$ for each bin in the Φ_r space, the simulated background is subtracted.

6.4 Particle flow ratio

Fig. 6.5 shows the bin-by-bin ratio of the charged particle flow in the *inside-W* over the charged particle flow in the *between-W* regions. The plot exhibits that the charged particle flow in the *between-W* regions is indeed raised stronger. The colour reconnection model is able to improve the simulation of the *ratio* of hadronic inter-jet activity. This indicates that the model qualitatively is working as expected.

For qualitative studies of the particle flow ratio it is convenient to define the ratio of the *inside-W* to the *between-W* particle flow by

$$R_N = \frac{\int_{0.2}^{0.8} d\Phi_r (dn_A + dn_C)/d\Phi_r}{\int_{0.2}^{0.8} d\Phi_r (dn_B + dn_D)/d\Phi_r}. \quad (6.3)$$

6.5 Summary

If we naively tune the model to the experimental value of R_N (by minimizing the log-likelihood function for p_{reco}), we obtain $p_{\text{reco}} = 1$ as the optimal value. However, R_N is not a very meaningful observable since it completely hides the fact that the absolute amount of particle flow exceeds the experimental data. Hence a model tuning at this stage does not make sense until the reasons for the excessive inter-jet hadron production are understood.

We find that colour reconnection affects the particle flow only to a small degree. The hadron production in the case of a moderate reconnection probability of $p_{\text{reco}} = 1/9$ is nearly the same as without colour reconnection. Even in the exaggerated case, $p_{\text{reco}} = 1$, the changes are not striking. In summary, the colour reconnection effect is too small to compensate for the difference between simulation and data.

6.6 Model investigation

In this section the charged particle flow observable is utilized to examine the spacetime-based colour reconnection model in more detail. First, the influence of the parton shower on the particle flow observable is studied. The section concludes with the comparison to other colour reconnection scenarios.

6.6.1 Initial parton shower evolution scale

To understand the exaggerated hadronic activity in the inter-jet regions, it is inevitable to look at the proceeding of the parton shower itself. There is the possibility to artificially suppress the initial parton shower evolution scale,

$$\tilde{q}_h \rightarrow y\tilde{q}_h,$$

where y is a real number between 0 and 1.

The idea is that parton branchings in the shower algorithm of **Herwig++** are *angular ordered* [44]. Emissions with larger angles occur at large evolution scales \tilde{q} at the beginning of the parton shower, whereas small evolution scale parameters at the end of the showering correspond to small angles between the branching products. By reducing the initial evolution scale, branchings at high scales are cut out. Thereby, the large angle part of the shower is reduced and branchings with small angles dominate. In doing so, one should be able to achieve a stronger collimation of jets.

However, the suppression of the initial scale is an academic example. The initial evolution scale \tilde{q}_h for the parton shower algorithm depends on the colour flow in the hard process, as mentioned in Sec. 3.3.1. It is calculated from the mass of the colour-connected partons and the energy scale Q^2 of the hard process [1], which is usually \hat{s} or \hat{t} . Multiplying \tilde{q}_h by an arbitrary factor lacks of any physical motivation. Thus the choice to rescale the initial scale can only be regarded as a facility to better understand the particle flow observable and hence the colour reconnection analyses at LEP2.

Moderate shower suppression (large y region)

In Fig. 6.6 the particle flow distribution for some *large* values of y is shown. Surprisingly, the angular spectrum shows almost no dependency on the initial evolution scale. This result suggests that the assumptions made above are too simplifying. Even if \tilde{q}_h is decreased, the maximum angle for the first branching is still given by the colour partner of the emitting parton (*cf.* Sec. 3.3.1). This is a possible reason why the particle flow at large angles with respect to the jet directions cannot be suppressed with this obvious method. In the case of success this could have been regarded as a hint

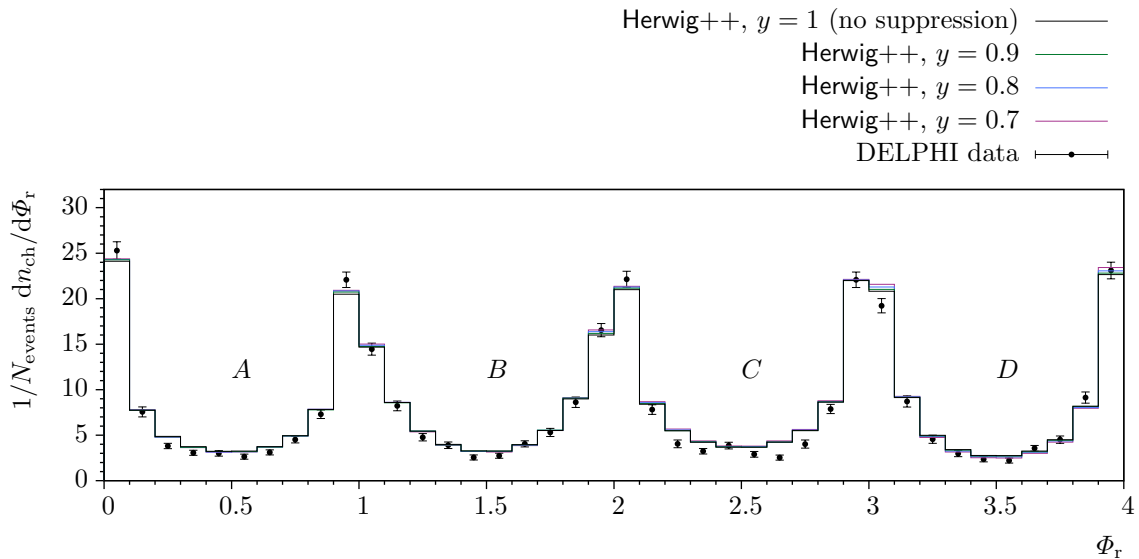


Fig. 6.6 Charged particle flow at 189 GeV: Several cases with moderate suppression of the initial evolution scale \tilde{q}_h are shown. This corresponds to large values of y . The changes in this observable are almost invisible.

that a tuning of p_{reco} , along with with other **Herwig++** parameters, can improve this observable. At the moment, however, this is only speculation.

Strong shower suppression (small y region)

For $y \lesssim 0.5$ the hadron production in the *inner-W* regions, *A* and *C*, increases strongly, as can be seen in Fig. 6.7. The reason is that with decreasing initial energy scale the forward emissions get more and more suppressed, too. The extreme scenario is $y = 0$: The parton shower evolution is completely suppressed, *i.e.* partonic decay products are combined to extremely heavy clusters with mass $m \approx M_W$. The hadron production is managed entirely by the non-perturbative cluster fission and decay model (*cf.* Sec. 3.4). It is therefore no surprise that the resulting distributions only give a poor description of the DELPHI data.

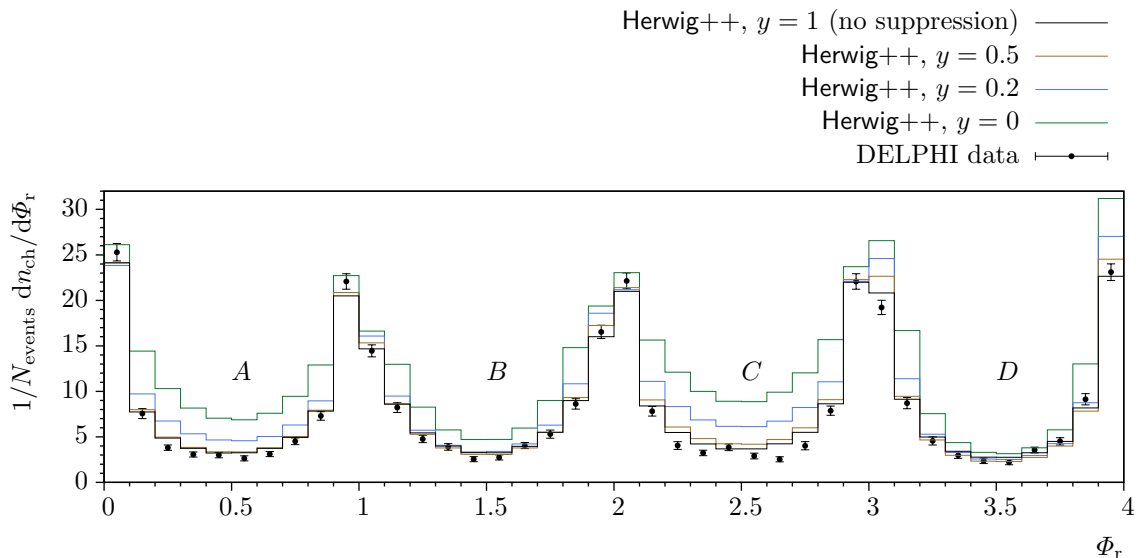


Fig. 6.7 The particle flow observable is affected significantly in the region of lower initial scales, *i.e.* smaller values of y .

6.6.2 A momentum space based model

For further insight into the impact of re-clustering on the particle flow, a slightly varied colour reconnection algorithm has been tested. Instead of basing on the event's spacetime structure, the varied algorithm follows a different approach: A reconnection of two clusters is possible, if this reduces the *invariant mass* of the clusters.

Recall (see Sec. 5.2.2) that the necessary condition for a re-clustering in the (spacetime-based) colour reconnection algorithm is

$$|d_{il}^2| + |d_{kj}^2| < |d_{ij}^2| + |d_{kl}^2|, \quad (5.5)$$

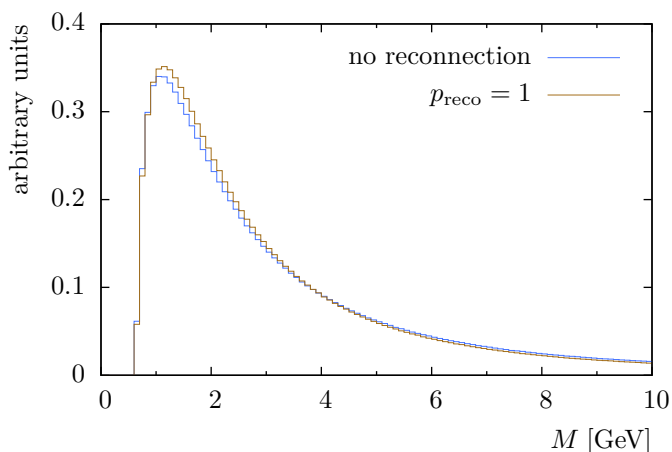


Fig. 6.8 Mass distribution of primary light clusters in e^+e^- collisions. The cluster mass distribution without reconnection (*cf.* Sec. 5.2.4) is compared to the extreme case $p_{\text{reco}} = 1$ in the momentum-based reconnection scheme.

motivated by the idea that the clustering of partons created nearby in spacetime is reasonable to be enhanced. In the modified model this requirement is replaced by

$$M_{il} + M_{kj} < M_{ij} + M_{kl}, \quad (6.4)$$

where $M_{ab}^2 = (p_a + p_b)^2$ is the (squared) invariant mass of the cluster consisting of the partons a and b . If for any pair of clusters an alternative clustering possibility can be found so that this requirement holds, the alternative is accepted with probability p_{reco} .

Clusters of partons nearby in momentum space are favoured by this model. This is a fairly generic modification of Herwig++'s usual cluster hadronization model. For instance, consider two partons that are close in momentum space. If they form a colour singlet state, it is natural to regard them as a (possibly excited) hadron state, in spite of any spacetime distances.

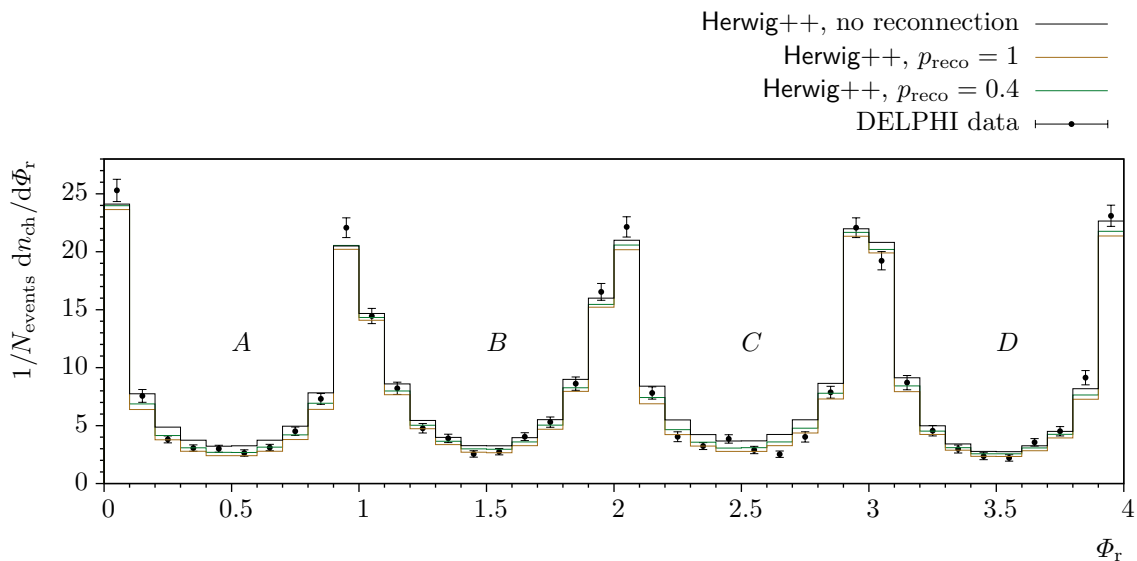


Fig. 6.9 Charged particle flow at 189 GeV, using the momentum-based colour reconnection model.

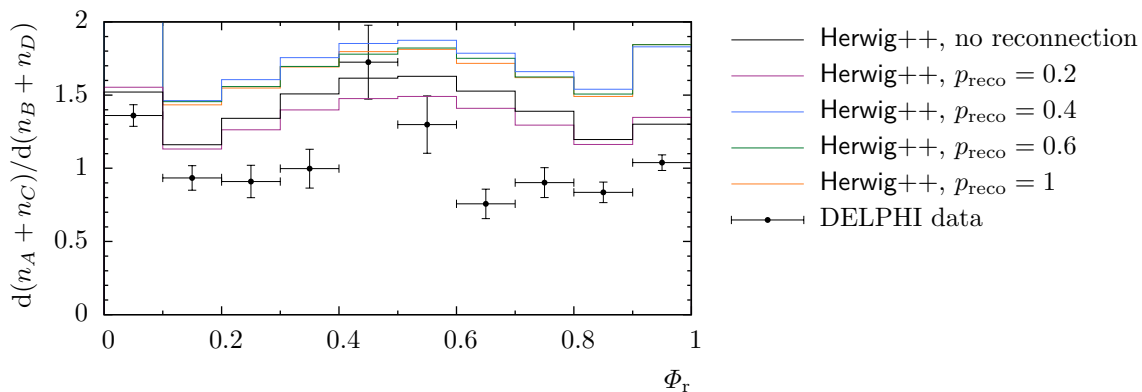


Fig. 6.10 Flow ratio simulation at 189 GeV of Herwig++ using the momentum-based colour reconnection model.

The cluster mass histograms in Fig. 6.8 show how the cluster mass spectrum is modified with this variant of colour reconnection. A slight shift to lower masses can be observed. However, the changes are not as severe as one might have expected thinking of the fact that the algorithm explicitly tries to reduce the cluster masses.

Note that colour octet clusters are prevented to be built, as in the case of the spacetime-based colour reconnection model. A narrow peak in the cluster mass spectrum, as in Fig. 5.8 in Sec. 5.2.4, would emerge here, too.

The impact in the charged particle flow observable is moderate. The multiplicity in all directions is slightly reduced. At first sight, this results in an improved description of the inter-jet activity.

The result may be an indicator that the application of this model in further test studies is worth being pursued. Further statements, relying on the basis of this single observable, cannot be made.

6.6.3 Random colour reconnection

Another benchmark test for the implemented colour reconnection model is the comparison to a toy model where the cluster formation is *randomized*. The creation of colour octet clusters is forbidden, as in the models before. Apart from that, every re-clustering possibility is allowed.

The particle flow observable is spoiled completely, as can be seen in Fig. 6.11. This indicates that changes in Herwig++'s existing hadronization model have to be done carefully. An arbitrary clustering scheme is unreasonable from a phenomenological point of view.

This result is connected to the *pre-confinement* property of QCD parton showers. The evolution to the cut-off scale Q_0 ends up in a stage consisting of colourless parton combinations with finite mass of $\mathcal{O}(Q_0)$ [50]. These colour singlets can be regarded

as pre-hadronic states, whose formation is predetermined by the parton shower. Only small corrections to this clustering possibility seem to be valid.

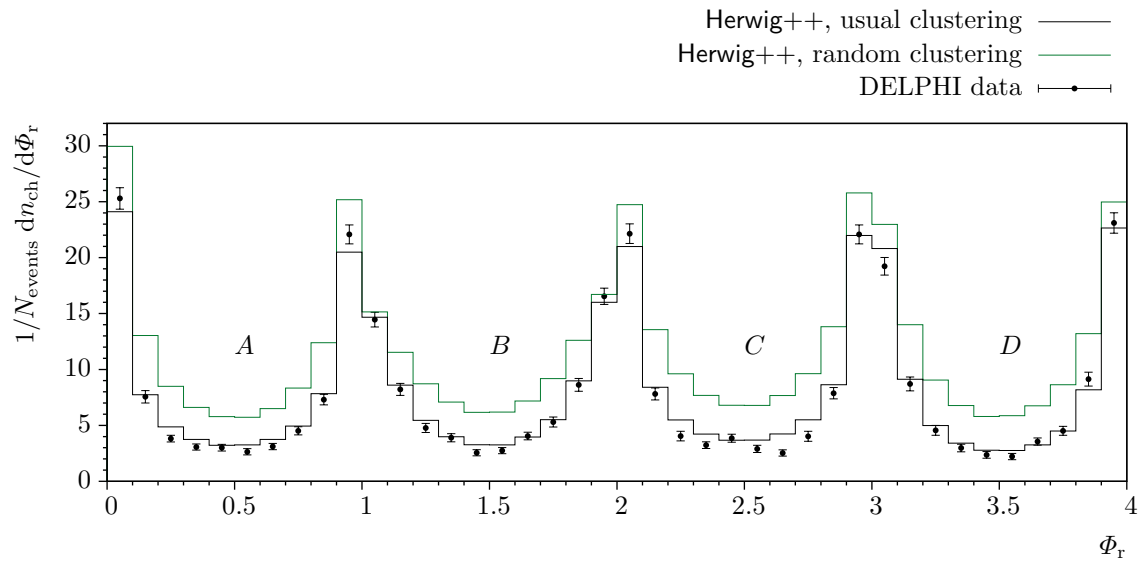


Fig. 6.11 Charged particle flow at 189 GeV, where partons are randomly clustered.

7 Outlook: Underlying event at the Tevatron

7.1 Introduction

The focus of current research in particle physics is certainly on hadron colliders, like the Tevatron or the recently launched *Large Hadron Collider* (LHC). In this sense, the development of `Herwig++` aims at an accurate simulation of hadron collisions. A proper handling of (well understood) lepton collisions is a necessary condition for that.

In order to find ‘new’ physics at the LHC, an accurate simulation of the standard model is inevitable. This includes a good description of the signal related to the hard subprocess. Moreover, additional (semi-hard) scatterings as well as the evolution of beam remnants at soft scales – both in common referred to as the *underlying event* – need to be modelled as precisely as possible. These effects are responsible for an unavoidable background for many observables.

At first, a short introduction on the role of colour reconnection (CR) in the simulation of the underlying event is given. The chapter concludes with a look at the impact of the new CR model on the simulation of certain observables measured at the Tevatron. However, the presented studies are performed on a qualitative level only. A tuning of the model, in the sense of minimizing χ^2 per degree of freedom, is not performed. Hence this chapter can only be regarded as an *outlook*.

7.2 Colour connections in hadron collisions

`Herwig++` makes use of a multi-parton interaction model [51] for the simulation of the underlying event. Technically, additional jets are achieved by the generation of secondary (semi-hard) subprocesses (see Sec. 3.5.1). As in the case of the hard subprocess, the scattering partons are extracted from the hadrons via a backward evolution from the (semi-)hard scale of the subprocess to hadronic scales. This evolution is forced to end up in a gluon which is extracted from the hadron remnant.

Colour connections between the additional initial-state showers emerge, as can be seen in Fig. 3.2. There is even the possibility that the colour connection stretches up to the final state parton shower. Recall that the maximum opening angle of a parton shower depends on the direction of the colour-connected parton¹. This implies that

the underlying event should be sensitive to the way these colour connections are set up during the extraction from the remnant. Currently this happens without a specific ordering [22]. The usage of an alternative colour connection model at this stage, e.g. via an ordering in the transverse momentum of the subprocesses, might affect the underlying event simulation.

It is not clear to what extent this net of colour connections, spanning major parts of the collision, is reasonable. The subprocesses, namely, can be assumed to be spread over hadronic distances. This makes a crosstalk between them quite improbable, at least in the highly perturbative regime. The presence of CR could help to improve the underlying event simulation. However, the present colour reconnection implementation acts at the non-perturbative stage *after* the evolution of all parton showers. It is thus possible that the impact of this model is minor, similar to the small effects observed at LEP in Ch. 6.

7.3 Underlying event in $p\bar{p}$ collisions at 1.8 TeV

A comparison to CDF data from Ref. [38] is performed. This analysis surveys events with charged particle jets in $p\bar{p}$ collisions at Tevatron Run I (at 1.8 TeV). The analysis is done with the help of Rivet [52], which is a tool for the validation and tuning of Monte Carlo event generators. The name of this analysis in Rivet is CDF_2001_S4751469.

The analysis is based on the partitioning of the $\eta - \phi$ space into “toward”, “away” and “transverse” regions. For each event these regions are defined individually as indicated in Fig. 7.1. The azimuthal angle ϕ is measured in the plane perpendicular to the beam axis, and η is the pseudorapidity in beam direction. The “towards” region is dominated by the hard process because it is chosen to contain the leading (*i.e.* hardest) jet. Because of momentum balance in the matrix element, the hard process is also responsible for the majority of the jet activity in the “away” region. The region most sensitive to the modelling of the underlying event is the “transverse” region.

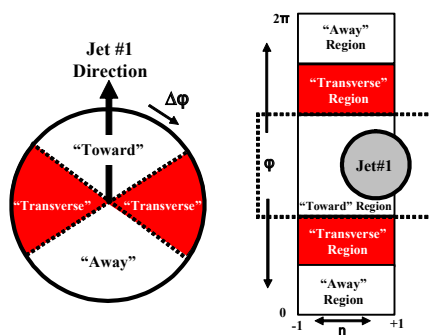


Fig. 7.1 Sketch of the “toward”, “transverse” and “away” regions in $\eta - \phi$ space, where ‘Jet #1’ is the hardest jet. The “transverse” region is defined by $60^\circ < |\Delta\phi| < 120^\circ$ and $|\eta| < 1$. Taken from Ref. [53].

¹ See Sec. 3.3 for an overview of the parton shower generation in Herwig++.

The experimental data are divided into two samples. The p_{\perp} of the leading jet ranges from 0 – 20 GeV for the *min-bias* sample and from 18 – 49 GeV for the *JET20* sample. The *min-bias* data were collected with a minimum set of cuts. Because of the high rate, however, the acceptance is reduced. In order to obtain many hard scattering events, the *JET20* trigger accepts only events with at least 20 GeV in a cluster of calorimeter cells.

7.3.1 The “transverse” region

The average number of charged particles in the “transverse” region approximately forms a plateau for $p_{\perp}^{\text{lead}} \gtrsim 5$ GeV, as displayed in Fig. 7.2. This can be seen as an indication that the activity in that region is indeed uncorrelated to the hard scattering process and hence can be used as a measure for the underlying event. However, *Herwig++* generates a small residual correlation between the hard scatter and the underlying event: The scalar sum of the transverse momenta, p_{\perp}^{sum} , in the “transverse” region slowly rises with p_{\perp}^{lead} , see Fig. 7.3.

Non-perturbative colour reconnection slightly enhances the charged particle multiplicity in the “transverse” region. This enhancement is independent of p_{\perp}^{lead} . One can also observe a small increase in p_{\perp}^{sum} in the “transverse” region (Fig. 7.3). The residual slope in the p_{\perp}^{sum} histogram is unaffected by colour reconnection. However, the changes are marginal, both in $\langle N_{\text{ch}} \rangle$ and in p_{\perp}^{sum} . The *uniform* increase in both observables exposes that CR dominantly affects the underlying event.

7.3.2 Dependency on the hadron radius

The spacetime points of multiple subprocesses are sampled using a parameter $1/\mu$ that can be interpreted as the radius of the colliding hadrons (*cf.* Sec. 5.1). Note that this parameter is independent of the hadron radius used in *Herwig++*’s multiple parton interaction model (MPI), which is therefore denoted as $1/\mu_{\text{MPI}}$ in this chapter.

In order to gain a better understanding of colour reconnection in the underlying event simulation, the dependency on the model parameters, *e.g.* the hadron radius, must be probed. A first step in that direction is done in Fig. 7.4. It compares $\langle N_{\text{ch}} \rangle$ for two (reasonable) values of the hadron radius, $1/\sqrt{0.71 \text{ GeV}^2}$ and $1/\sqrt{2 \text{ GeV}^2}$. This observable turns out to be invariant in this (limited) region of the parameter space.

7.3.3 Momentum-space colour reconnection

The usage of the momentum-space CR model (*cf.* Sec. 6.6.2) yields more promising results, as can be seen in Figs. 7.5 and 7.6. In the small p_{\perp}^{lead} region, both $\langle N_{\text{ch}} \rangle$ and p_{\perp}^{sum} are described ‘well’ for $p_{\text{reco}} \approx 0.3$. For large p_{\perp}^{lead} , an improvement can be seen only for $\langle N_{\text{ch}} \rangle$. It is also interesting to see that the impact on $\langle N_{\text{ch}} \rangle$ and p_{\perp}^{sum} seems

to be uncorrelated. *I.e.* these observables scale differently with p_{reco} (in the high- p_{\perp}^{lead} region), whereas the spacetime CR model shows a uniform scaling.

7.3.4 Conclusion

These first tests did not reveal that *spacetime-based* colour reconnection causes severe changes in the simulation of the underlying event. Furthermore, it seems not to be able to improve the poor simulation in the low p_{\perp}^{lead} region. This issue, of course, requires further systematic studies. It will be an important task to test the behaviour of the model in extreme scenarios, which can be understood as a validation process. A systematic tuning of MPI and CR model parameters might answer the question whether this CR model needs to be modified for the usage in hadron collisions.

The *momentum-based* CR model, however, seems to be quite successful. It enables an enhanced description of the underlying event. Additionally, the model has the advantage of having only one free parameter, p_{reco} .

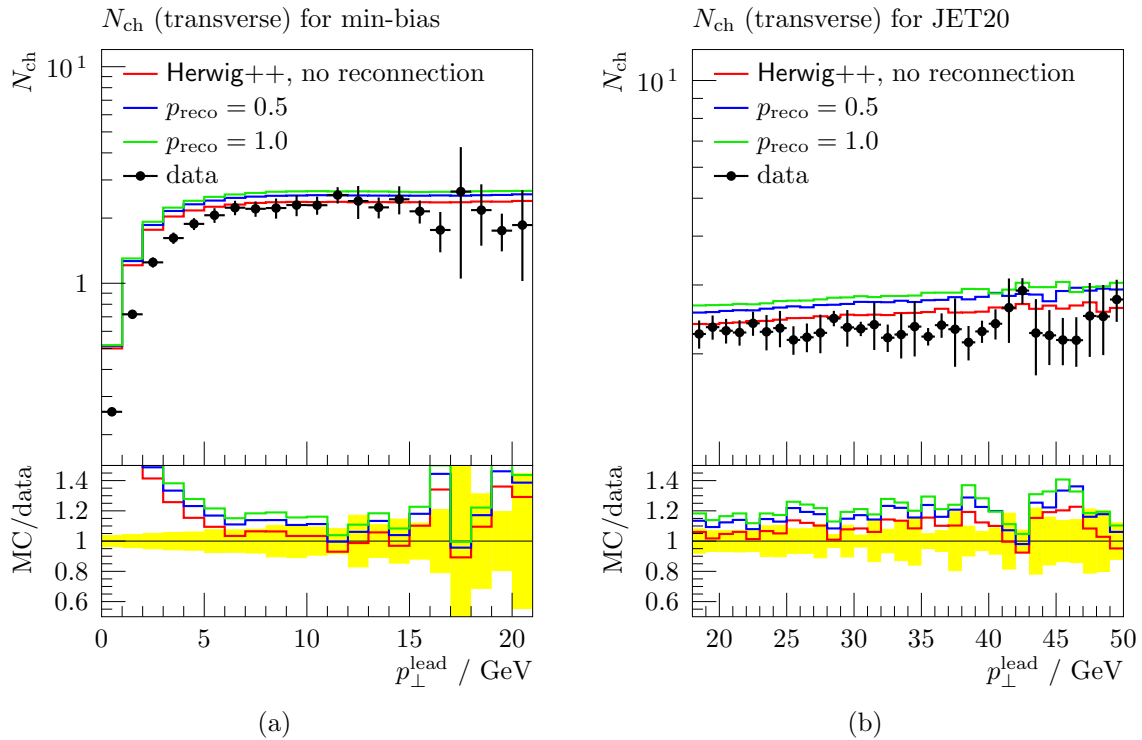


Fig. 7.2 Average number of charged particles in the “transverse” region. The MPI model uses its default settings: The squared inverse hadron radius is $\mu_{\text{MPI}}^2 = 1.2 \text{ GeV}^2$ and the minimal transverse momentum of additional scatters is set to $p_t^{\text{min}} = 4.3 \text{ GeV}$.

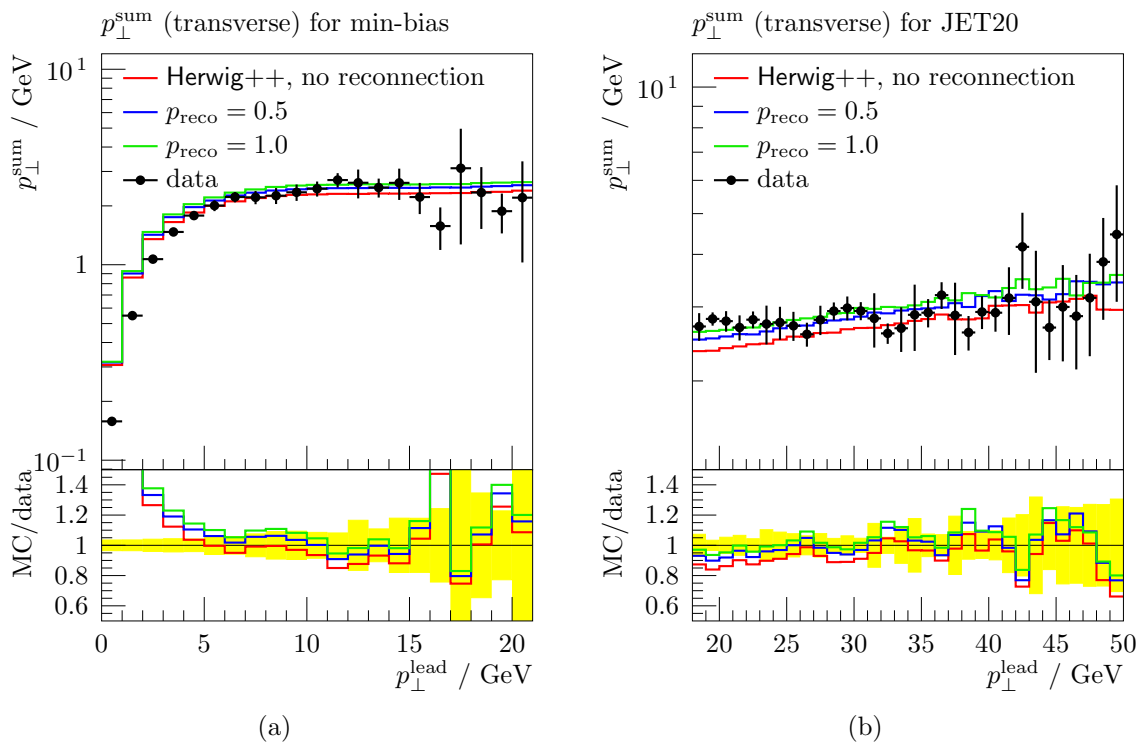


Fig. 7.3 p_{\perp}^{sum} in the “transverse” region. The MPI settings are as in Fig. 7.2.

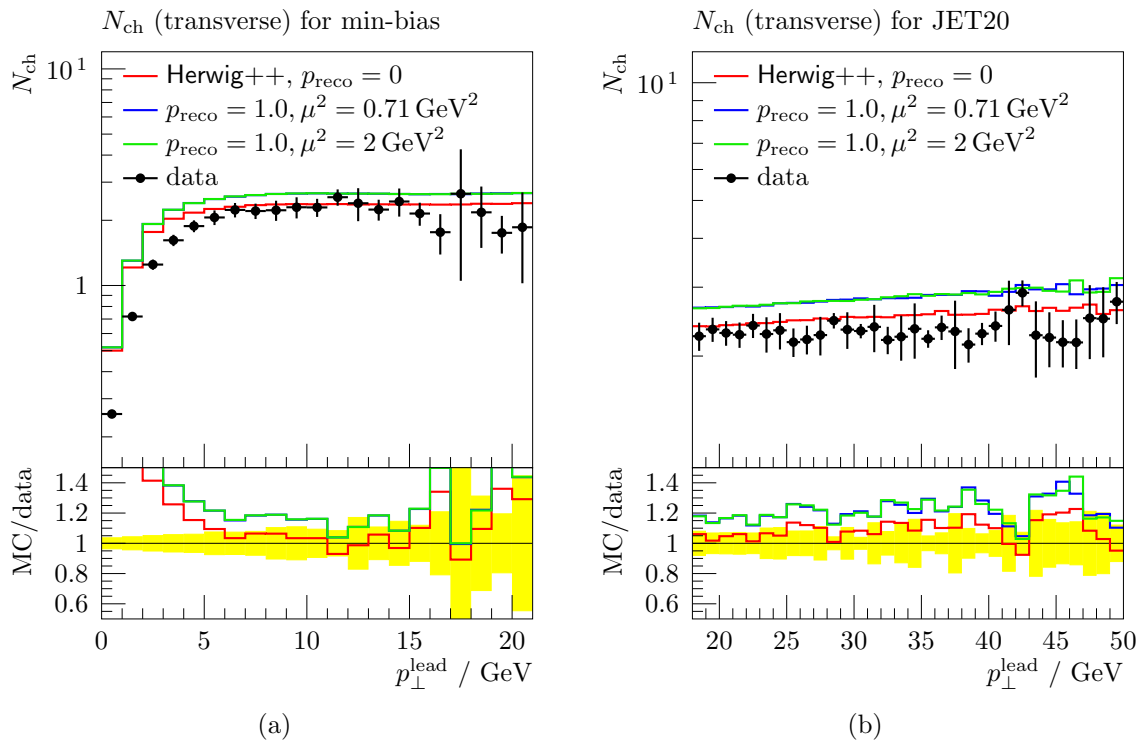


Fig. 7.4 For the two probed values of the squared inverse hadron radius μ^2 there is no difference recognizable. Note that this is **not** the hadron radius parameter of the MPI model, $1/\mu_{\text{MPI}}$. The MPI settings are as in Fig. 7.2.

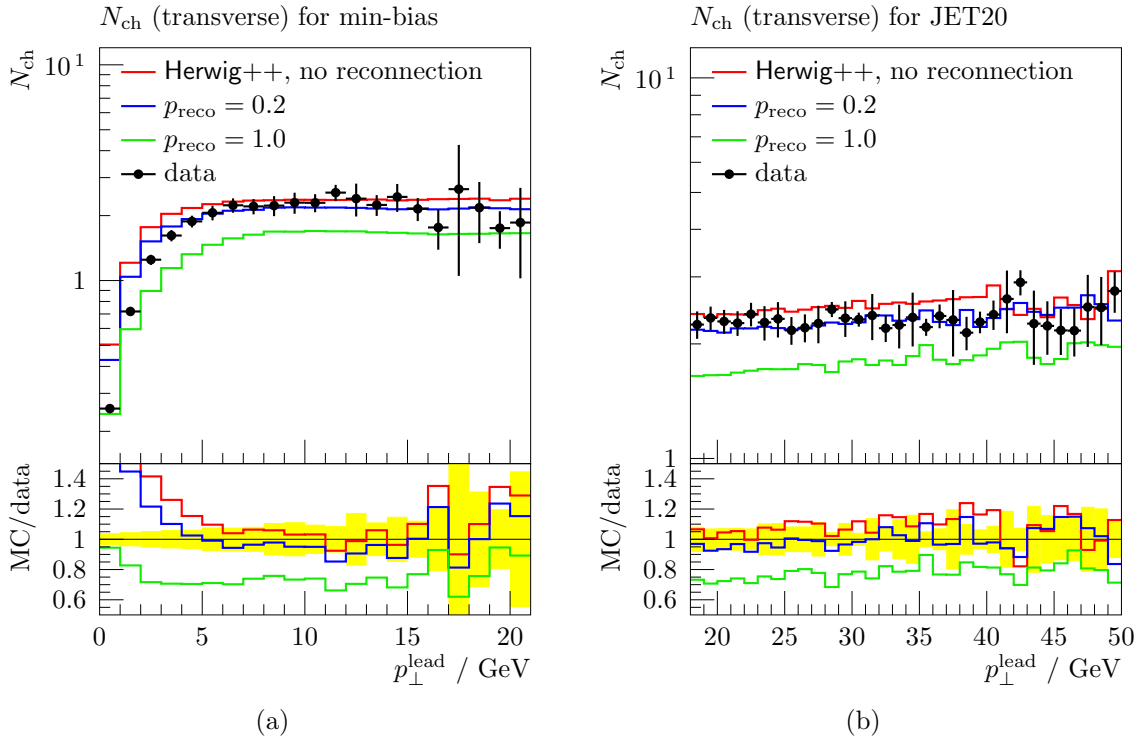


Fig. 7.5 Average number of charged particles in the “transverse” region, using the **momentum-space** colour reconnection model.

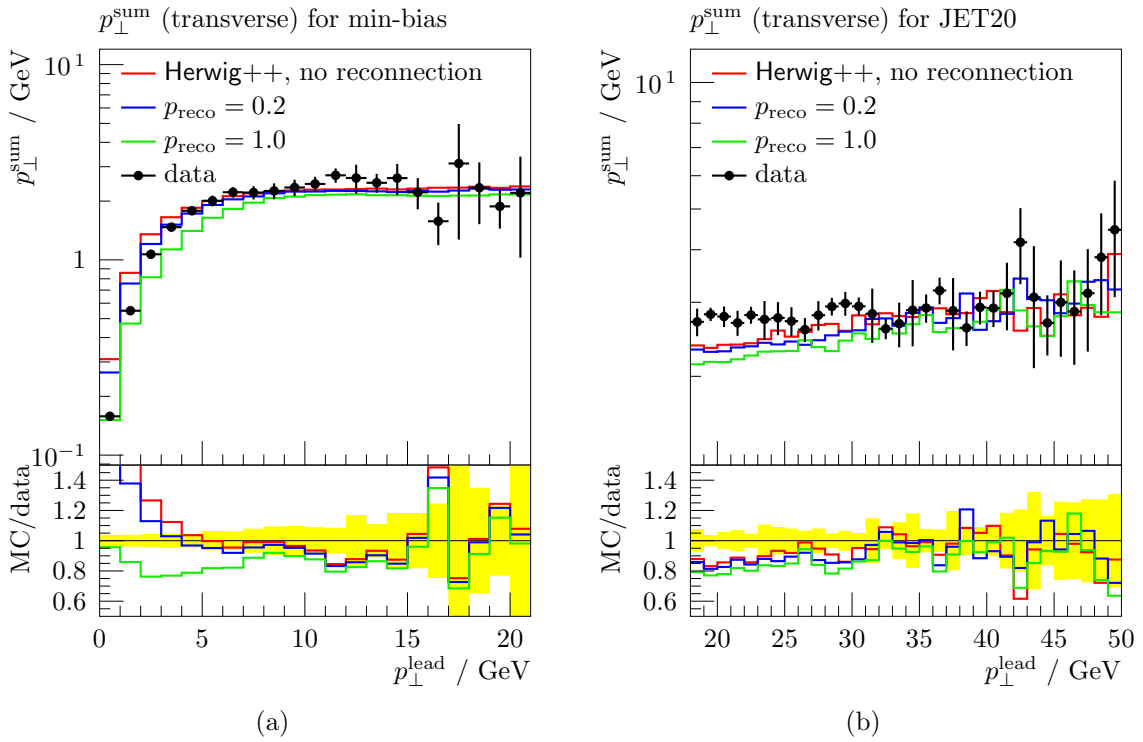


Fig. 7.6 p_{\perp}^{sum} in the “transverse” region with the **momentum-space** colour reconnection model.

8 Summary and conclusions

The aim of this work was to provide the possibility of colour reconnection in the event generator **Herwig++**. The model had to be tested and validated in the description of hadronic W pair decays at LEP. Moreover, a tuning to LEP data was contemplated in order to achieve a starting point for a model that is able to improve the description of the underlying event in hadron collisions.

A colour reconnection implementation in **Herwig++** has been accomplished. The model is inspired by an existing implementation in the event generator **HERWIG** [2]. It intervenes the hadronization process by allowing a recreation of clusters, which can be regarded as pre-hadronic states. The untouched hadronization model generates clusters from partons which are colour-connected according to their history in the subprocess and parton shower generation. The colour reconnection model modifies this procedure by allowing partons to cluster which are nearby in spacetime.

In order to equip the partons with spacetime information, a spacetime model has been assembled and implemented. It is able to handle multiple parton interactions in hadron collisions, relying on an estimation for the spatial parton density.

A detailed analysis of the particle flow in $WW \rightarrow 4\text{jets}$ events has been performed. Regarding the sensitivity to colour reconnection effects, this is the most prominent observable and has been studied extensively by the LEP Collaborations. The spacetime overlap of the hadronization regions of the two hadronically decaying W bosons gives rise to expect effects descending from a common hadronization phase. The unchanged **Herwig++** simulation exhibits systematic deviations from experimental data in the particle flow observable. Colour reconnection, however, has been shown to cause only small changes, which cannot compensate for the differences between simulation and experimental data. Hence a tuning to data could not be accomplished although the model qualitatively is working as expected.

The origin of the inaccurate simulation was suspected to be located in the parton shower. Bearing this in mind, a gradual suppression of large-angle emissions in the parton shower was tested. The particle flow observable was expected to be biased by this suppression. However, this could not be observed.

In order to make sense of this puzzle, modifications in the colour reconnection model were considered. Regarding this, the spacetime based colour reconnection model has been compared to an alternative reconnection model, which favours clusters of partons nearby in *momentum space*. This alternative model has been found to improve the simulation of the particle flow observable.

Finally, the impact of colour reconnection on the underlying event in hadron collisions has been examined. Because this last analysis is far from detailed, it serves as an outlook only. In particular, the mean charged multiplicity $\langle N_{\text{ch}} \rangle$ and the sum of the scalar transverse momenta p_{\perp}^{sum} in the so-called ‘transverse’ region have been analyzed, based on data from the CDF experiment at the Tevatron. This region in η - ϕ space is defined by the direction of the hardest jet in the event. $\langle N_{\text{ch}} \rangle$ and p_{\perp}^{sum} , restricted to the particles in the ‘transverse’ region, can be utilized as a measure for the underlying event.

In brief, both $\langle N_{\text{ch}} \rangle$ and p_{\perp}^{sum} are increased uniformly by the existence of *spacetime-based* colour reconnection, regardless of the transverse momentum of the hardest jet. Furthermore, the impact on both observables seems to be correlated.

In contrast, underlying event simulation using the *momentum-based* colour reconnection model yields more promising results. As a rough estimate, the agreement between simulation and experimental data is improved by this model using a moderate reconnection probability. Moreover, $\langle N_{\text{ch}} \rangle$ and p_{\perp}^{sum} are changed in a more decorrelated way.

This thesis serves as a starting point for future colour reconnection studies. The tools that have been implemented within this work provide the opportunity to improve the predictive value of **Herwig++**. However, both the spacetime-based and the momentum-based model are not yet ready for use. Further test studies will show if one of these models will find its way into **Herwig++**’s default repertoire. Concerning the underlying event simulation, the latter model seems to deserve special attention – despite being rather a spin-off.

A Sampling of scattering centres

This chapter outlines how the x and y components of the spacetime point of a hard sub-process in hadronic collisions are sampled according to the spatial partonic probability density

$$A_\mu(b) = \frac{\mu^2}{96\pi} (\mu b)^3 K_3(\mu b). \quad (\text{A.1})$$

In this equation, μ has energy dimension 1 and $b = \sqrt{x^2 + y^2}$ is the distance from the origin in the x - y plane. K_3 is the modified Bessel function of the third kind. $A_\mu(b)$ is normalized to unity in x - y space,

$$\int d^2\mathbf{b} A_\mu(b) = 1. \quad (\text{A.2})$$

For simplicity, we change to polar coordinates, $(x, y) \mapsto (r, \varphi)$. Since A_μ is rotationally symmetric, the polar angle φ is chosen flat in $(0, 2\pi)$ and Eq. (A.2) simply reads

$$\int_0^\infty db 2\pi b A_\mu(b) = 1. \quad (\text{A.3})$$

The remaining task is to sample the radius b from the radial density

$$f_\mu(b) \equiv 2\pi b A_\mu(b). \quad (\text{A.4})$$

Because a primitive of f_μ is not known, we have to find an overestimate g_μ which satisfies

$$g_\mu(b) \geq f_\mu(b) \quad \text{for all } b \in [0, \infty), \quad (\text{A.5})$$

and for which, additionally, a primitive $\int g_\mu(b) db$ can be found.

The algorithm to choose b according to $f_\mu(b)$ is then:

- (1) Choose b from $g_\mu(b)$ by solving

$$\mathcal{R}_1 = \frac{\int_0^b dz g_\mu(z)}{\int_0^\infty dz g_\mu(z)}, \quad (\text{A.6})$$

where \mathcal{R}_1 is chosen flat from $(0, 1)$.

- (2) Choose another random number \mathcal{R}_2 , flat in $(0, 1)$.
If $\mathcal{R}_2 < \frac{f_\mu(b)}{g_\mu(b)}$, accept b , else go back to step (1).

It has been found that a Breit-Wigner-like function

$$g_\mu(b) = \frac{a}{(b-c)^2 + d} \quad (\text{A.7})$$

satisfies condition (A.5), where

$$\begin{aligned} a &= 0.7907 \text{ fm}, \\ c &= c(\mu) = \frac{0.46106}{\sqrt{\mu^2 / \text{GeV}^2}} \text{ fm}, \\ d &= d(\mu) = \frac{0.6961}{\sqrt{\mu^2 / \text{GeV}^2}} \text{ fm}^2. \end{aligned} \quad (\text{A.8})$$

A general proof that this choice for an overestimate holds for $\mu \in (0, \infty)$ has not been performed. However, g_μ has been shown to be valid at least for not too extreme parameters, $\mu^2 = 0.1 \dots 10 \text{ GeV}^2$. Note that the default value is $\mu^2 = 0.71 \text{ GeV}^2$.

With this overestimate, the solution of Eq. (A.6) is

$$b = c + \sqrt{d} \tan \left[\mathcal{R}_1 \left(\frac{\pi}{2} + \arctan \frac{c}{\sqrt{d}} \right) - \arctan \frac{c}{\sqrt{d}} \right]. \quad (\text{A.9})$$

(Almost) needless to say, the re-transformation to Cartesian coordinates is generically

$$(\varphi, b) \mapsto \begin{pmatrix} x \\ y \end{pmatrix} = b \begin{pmatrix} \cos \varphi \\ \sin \varphi \end{pmatrix}. \quad (\text{A.10})$$

B Lifetime of virtual partons

A particle with mass m and 4-momentum q_μ is referred to as *virtual* (off mass-shell) if

$$q_\mu q^\mu \equiv q^2 \neq m^2. \quad (\text{B.1})$$

In this section an expression for the mean lifetime of a virtual particle as a function of its virtuality q^2 is derived.

Consider a virtual particle at rest¹ ($\mathbf{q} = 0$). Its energy $E = \sqrt{q^2}$ differs from its rest mass that fixes the energy \tilde{E} of the real particle via $\tilde{E}^2 = m^2$. Further, let this particle be stable in its real state, *i.e.* let its width Γ vanish initially.

The mean lifetime can be assessed, as similarly done in Ref. [54], via Heisenberg's uncertainty principle

$$\tau \cdot \Delta E \approx \frac{\hbar}{2}, \quad (\text{B.2})$$

where the energy difference is given by $\Delta E = |\tilde{E} - E| = |\sqrt{q^2} - m|$. Hence we find for an off-shell particle with no natural width

$$\tau_{\text{no width}}(q^2) = \frac{\hbar}{2} \frac{1}{|\sqrt{q^2} - m|}. \quad (\text{B.3})$$

Apparently, this expression diverges for $q^2 \rightarrow m^2$, which is the limit where the particle returns to its mass-shell again. This is reasonable because a real particle without natural width is indeed stable.

Let us now consider the case of a particle whose width is non-vanishing. On mass-shell the mean lifetime is given by

$$\tau_0 = \frac{\hbar}{\Gamma}, \quad (\text{B.4})$$

whereas far off mass-shell we can regard Eq. (B.3) as an appropriate approximation for the lifetime because in highly virtual momentum regions Γ is negligible compared to ΔE .

$$\tau(q^2) = \frac{\hbar}{\sqrt{4(\sqrt{q^2} - m)^2 + \frac{\Gamma^2 q^2}{m^2}}}. \quad (\text{B.5})$$

interpolates between Eq. (B.3) and Eq. (B.4). Fig. 5.2 at Page 24 shows $\tau(q^2)$ and $\tau_{\text{no width}}(q^2)$ in one plot.

¹ This restriction implies that the particle's momentum is time-like, $q^2 > 0$, because otherwise it is impossible to boost to a Lorentz frame where $\mathbf{q} = 0$ holds.

C Model parameters

This appendix summarizes the parameters used by the spacetime-based colour reconnection model. A detailed depiction of the code structure, however, is pointless at this place since a major refactoring is planned before the code is released.

- **MinimumVirtuality**
To prevent the travelling distances of partons from getting too large, this parameter is used as a lower limit on their virtuality. The default value is 0.5 GeV.
- **InvRadiusSquared**
The squared inverse hadron radius μ^2 , used for the sampling of the spacetime point of multiple scattering centres during one hadron collision. This is a free parameter and not (yet) connected to μ^2 in the multiple interaction model.
- **ReconnectionProbability**
The probability p_{reco} that a found reconnection possibility is actually accepted.

Bibliography

- [1] M. Bähr *et al.*, *Herwig++ Physics and Manual*. Eur. Phys. J. **C58** (2008) 639–707, arXiv:0803.0883 [hep-ph].
- [2] G. Marchesini *et al.*, *HERWIG version 5.9: A Monte Carlo event generator*. arXiv:hep-ph/9607393.
- [3] T. Muta, *Foundations of quantum chromodynamics: An Introduction to perturbative methods in gauge theories*. World Sci. Lect. Notes Phys. **5** (1987) 1–409.
- [4] D. J. Gross and F. Wilczek, *Ultraviolet Behavior of Non-abelian Gauge Theories*. Phys. Rev. Lett. **30** (1973) 1343–1346.
- [5] H. D. Politzer, *Reliable Perturbative Results for Strong Interactions?* Phys. Rev. Lett. **30** (1973) 1346–1349.
- [6] R. K. Ellis, W. J. Stirling, and B. R. Webber, *QCD and collider physics*. Camb. Monogr. Part. Phys. Nucl. Phys. Cosmol. **8** (1996) 1–435.
- [7] K. G. Wilson, *Confinement of Quarks*. Phys. Rev. **D10** (1974) 2445–2459.
- [8] V. Barger and R. Phillips, *Collider physics*. Frontiers in physics ; 71. Addison-Wesley, Redwood City, Calif., 1987.
- [9] A. Bassetto, M. Ciafaloni, G. Marchesini, and A. H. Mueller, *Jet Multiplicity and Soft Gluon Factorization*. Nucl. Phys. **B207** (1982) 189.
- [10] Y. L. Dokshitzer, V. S. Fadin, and V. A. Khoze, *Coherent Effects in the Perturbative QCD Parton Jets*. Phys. Lett. **B115** (1982) 242–246.
- [11] B. I. Ermolaev and V. S. Fadin, *Log - Log Asymptotic Form of Exclusive Cross-Sections in Quantum Chromodynamics*. JETP Lett. **33** (1981) 269–272.
- [12] G. Marchesini and B. R. Webber, *Simulation of QCD Jets Including Soft Gluon Interference*. Nucl. Phys. **B238** (1984) 1.
- [13] G. Marchesini *et al.*, *HERWIG: A Monte Carlo event generator for simulating hadron emission reactions with interfering gluons. Version 5.1 - April 1991*. Comput. Phys. Commun. **67** (1992) 465–508.
- [14] F. Maltoni and T. Stelzer, *MadEvent: Automatic event generation with MadGraph*. JHEP **02** (2003) 027, arXiv:hep-ph/0208156.

- [15] K. Arnold *et al.*, *VBFNLO: A parton level Monte Carlo for processes with electroweak bosons*. Comput. Phys. Commun. **180** (2009) 1661–1670, arXiv:0811.4559 [hep-ph].
- [16] E. Boos *et al.*, *Generic user process interface for event generators*. arXiv:hep-ph/0109068.
- [17] J. Alwall *et al.*, *A standard format for Les Houches event files*. Comput. Phys. Commun. **176** (2007) 300–304, arXiv:hep-ph/0609017.
- [18] T. Sjöstrand, S. Mrenna, and P. Z. Skands, *A Brief Introduction to PYTHIA 8.1*. Comput. Phys. Commun. **178** (2008) 852–867, arXiv:0710.3820 [hep-ph].
- [19] T. Gleisberg *et al.*, *Event generation with SHERPA 1.1*. JHEP **02** (2009) 007, arXiv:0811.4622 [hep-ph].
- [20] S. Gieseke, P. Stephens, and B. Webber, *New formalism for QCD parton showers*. JHEP **12** (2003) 045, arXiv:hep-ph/0310083.
- [21] G. Marchesini and B. R. Webber, *Monte Carlo Simulation of General Hard Processes with Coherent QCD Radiation*. Nucl. Phys. **B310** (1988) 461.
- [22] M. Bähr, S. Gieseke, and M. H. Seymour, *Simulation of multiple partonic interactions in Herwig++*. JHEP **07** (2008) 076, arXiv:0803.3633 [hep-ph].
- [23] G. 't Hooft, *A planar diagram theory for strong interactions*. Nucl. Phys. **B72** (1974) 461.
- [24] B. R. Webber, *A QCD Model for Jet Fragmentation Including Soft Gluon Interference*. Nucl. Phys. **B238** (1984) 492.
- [25] G. Corcella *et al.*, *HERWIG 6.5: an event generator for Hadron Emission Reactions With Interfering Gluons (including supersymmetric processes)*. JHEP **01** (2001) 010, arXiv:hep-ph/0011363.
- [26] CDF Collaboration, F. Abe *et al.*, *Double parton scattering in $\bar{p}p$ collisions at $\sqrt{s} = 1.8\text{TeV}$* . Phys. Rev. **D56** (1997) 3811–3832.
- [27] M. Bähr, J. M. Butterworth, S. Gieseke, and M. H. Seymour, *Soft interactions in Herwig++*. arXiv:0905.4671 [hep-ph].
- [28] T. Sjöstrand and V. A. Khoze, *On Color rearrangement in hadronic W^+W^- events*. Z. Phys. **C62** (1994) 281–310, arXiv:hep-ph/9310242.
- [29] G. Gustafson, U. Pettersson, and P. M. Zerwas, *Jet Final States in $W W$ Pair Production and Color Screening in the QCD Vacuum*. Phys. Lett. **B209** (1988) 90.
- [30] B. R. Webber, *Colour reconnection and Bose-Einstein effects*. J. Phys. **G24** (1998) 287–296, arXiv:hep-ph/9708463.
- [31] LEP Collaboration, R. Strohmer, *Bose-Einstein correlations and color reconnection in hadronic W* . PoS **HEP2005** (2006) 304, arXiv:hep-ex/0601015.

- [32] **DELPHI** Collaboration, J. Abdallah *et al.*, *Investigation of Colour Reconnection in WW Events with the DELPHI detector at LEP-2*. Eur. Phys. J. **C51** (2007) 249–269, [arXiv:0704.0597 \[hep-ex\]](#).
- [33] **L3** Collaboration, P. Achard *et al.*, *Search for color reconnection effects in $e^+e^- \rightarrow W^+W^- \rightarrow$ hadrons through particle flow studies at LEP*. Phys. Lett. **B561** (2003) 202–212, [arXiv:hep-ex/0303042](#).
- [34] **ALEPH** Collaboration, T. Ziegler, *Colour reconnection studies using particle flow between W bosons at $\sqrt{s} = 189 - 208$ GeV*. ALEPH-2001-047.
- [35] **OPAL** Collaboration, G. Abbiendi *et al.*, *Colour reconnection in $e^+e^- \rightarrow W^+W^-$ at $\sqrt{s} = 189 - 209$ GeV*. Eur. Phys. J. **C45** (2006) 291–305, [arXiv:hep-ex/0508062](#).
- [36] D. Wicke and P. Z. Skands, *Non-perturbative QCD Effects and the Top Mass at the Tevatron*. [arXiv:0807.3248 \[hep-ph\]](#).
- [37] **CDF** Collaboration, R. D. Field, *Studying the underlying event at CDF*. Presented at 33rd International Conference on High Energy Physics (ICHEP 06), Moscow, Russia, 26 Jul - 2 Aug 2006.
- [38] **CDF** Collaboration, A. A. Affolder *et al.*, *Charged jet evolution and the underlying event in $p\bar{p}$ collisions at 1.8 TeV*. Phys. Rev. **D65** (2002) 092002.
- [39] D. Kar, R. Field, “Using Drell-Yan to Probe the Underlying Event in Run 2 at CDF.” CDF Note, CDF/PUB/CDF/PUBLIC/9351, 2008.
- [40] R. Field, “Jet Physics and the Underlying Event at the Tevatron.” CDF Note, CDF/PUB/CDF/PUBLIC/7898, 2008.
- [41] G. Gustafson, *Multiple scattering, underlying event, and minimum bias*. [arXiv:0712.1941 \[hep-ph\]](#).
- [42] R. C. Walker *et al.*, *Measurements of the proton elastic form-factors for $1 \text{ GeV}/c^2 \leq Q^2 \leq 3 \text{ GeV}/c^2$ at SLAC*. Phys. Rev. **D49** (1994) 5671–5689.
- [43] M. Bähr, *Underlying Event Simulation in the Herwig++ Event Generator*. PhD thesis, Universität Karlsruhe (TH), 2008. <http://digbib.ubka.uni-karlsruhe.de/volltexte/1000010075>.
- [44] S. Gieseke, A. Ribon, M. H. Seymour, P. Stephens, and B. Webber, *Herwig++ 1.0: An event generator for e^+e^- annihilation*. JHEP **02** (2004) 005, [arXiv:hep-ph/0311208](#).
- [45] D. Duchesneau, *New method based on energy and particle flow in $e^+e^- \rightarrow W^+W^- \rightarrow$ hadron events for color reconnection studies*. Presented at Workshop on WW Physics at LEP200 (WW99), Kolymbari, Chania, Greece, 20-23 Oct 1999.
- [46] P. Abreu *et al.*, *The estimation of the effective centre of mass energy in q anti- q gamma events from DELPHI*. Nucl. Instrum. Meth. **A427** (1999) 487–494, [arXiv:hep-ex/9809008](#).

- [47] S. Catani, Y. L. Dokshitzer, M. Olsson, G. Turnock, and B. R. Webber, *New clustering algorithm for multi-jet cross-sections in e^+e^- annihilation*. Phys. Lett. **B269** (1991) 432–438.
- [48] M. Cacciari and G. P. Salam, *Dispelling the N^3 myth for the k_t jet-finder*. Phys. Lett. **B641** (2006) 57–61, [arXiv:hep-ph/0512210](#).
- [49] D. Zeppenfeld, *Collider physics*. [arXiv:hep-ph/9902307](#).
- [50] D. Amati and G. Veneziano, *Preconfinement as a Property of Perturbative QCD*. Phys. Lett. **B83** (1979) 87.
- [51] M. Bähr, S. Gieseke, and M. H. Seymour, *Multiple Interactions in Herwig++*. [arXiv:0806.4250 \[hep-ph\]](#).
- [52] A. Buckley *et al.*, *Rivet user manual*. [arXiv:1003.0694 \[hep-ph\]](#).
- [53] **CDF** Collaboration, R. Field, *Jet physics and the underlying event at the Tevatron*. AIP Conf. Proc. **828** (2006) 163–174.
- [54] V. L. Lyuboshitz and V. V. Lyuboshitz, *Lifetime and Path Length of the Virtual Particle*. Physics of Atomic Nuclei **68** (2005) 524–527.

Zusammenfassung

Monte-Carlo-Ereignis-Generatoren spielen eine zentrale Rolle in der modernen Teilchenbeschleuniger-Physik. Sie werden für die Simulation von Endzuständen in Teilchenkollisionen benutzt, um einen Vergleich mit experimentell gemessenen Daten zu ermöglichen. Große Teile der Ereignis-Generierung basieren auf der Quantenchromodynamik (QCD), der Theorie der starken Wechselwirkung. Die fundamentalen Teilchen in dieser Theorie sind Gluonen, Quarks und Antiquarks – man spricht allgemein auch von Partonen.

In der Hochenergiephysik können Streuamplituden störungstheoretisch berechnet werden. Mit diesem Hilfsmittel lassen sich Streu-Ereignisse auf der Basis von Wahrscheinlichkeiten erzeugen. Jedoch können solche Endzustände nicht direkt beobachtet werden, die farbgeladene Teilchen, also Partonen darunter enthalten. Diese existieren nicht als freie Teilchen sondern werden nur in gebundenen Zuständen, den Mesonen und Baryonen (oder allgemein, den Hadronen), beobachtet. Diese bemerkenswerte Eigenschaft der QCD wird *Confinement* genannt.

Der Übergang vom partonischen Endzustand des harten Prozesses zu einem Zustand, der aus beobachtbaren Hadronen besteht, wird von Ereignis-Generatoren in zwei Schritten bewerkstelligt. Im ersten Schritt werden sogenannte Parton-Schauer erzeugt. Diese entspringen sorgfältigen Verfahren in der perturbativen QCD und berücksichtigen zusätzliche weiche und kollineare Abstrahlungen von den ausgehenden Partonen. Am Ende des Schauers, wo die Störungstheorie ihre Gültigkeit verliert, verbleibt ein Zustand vieler Partonen niedriger Energie-Skala. Im zweiten Schritt werden *Hadronisierungs-Modelle* dazu benutzt, den partonischen Zustand in einen hadronischen Endzustand überzuführen. Bestehende Hadronisierungs-Modelle versuchen, eine verlässliche Simulation experimenteller Beobachtungen zu bieten, wobei sie – aufgrund fehlender theoretischer Kenntnisse des Hadronisierungs-Prozesses – stark auf Phänomenologie basieren.

Ziel dieser Arbeit war es, ein sogenanntes *Colour-Reconnection-Modell* im Monte-Carlo-Ereignis-Generator **Herwig++** zu implementieren und zu untersuchen. Dieses Modell kann als Erweiterung zum bestehenden Hadronisierungs-Modell betrachtet werden. Es ermöglicht, den Austausch zusätzlicher weicher Gluonen in der nicht-perturbativen Hadronisierungs-Phase miteinzubeziehen. Das Colour-Reconnection-Modell wurde sowohl für die Simulation von Lepton- als auch von Hadron-Kollisionen entworfen. Es lehnt stark an eine bereits existierende Implementierung in **HERWIG** an, dem Vorgänger von **Herwig++**.

Dieses Modell sollte dann anhand der Simulation hadronischer W -Paar-Zerfälle getestet und validiert werden. Dafür stehen experimentelle Daten vom *Large-Electron-Positron-Collider*-Experiment (LEP) zur Verfügung. Schließlich sollte mit Hilfe dieser Analyse ein Tuning des Modells erfolgen, also eine möglichst gute Beschreibung der Daten erzielt werden. Zu guter Letzt war vorgesehen, von diesem Standpunkt aus eine Verbesserung der Simulation des sogenannten Underlying Events in Hadron-Kollisionen anzustreben. Ausgangspunkt dieses Vorhabens sind bestehende Defizite in der bisherigen Beschreibung des Underlying Events am Tevatron. Nicht zuletzt konzentrieren sich die momentanen Bemühungen in Richtung des *Large Hadron Colliders* (LHC), wo eine vorhergesagte kräftige Simulation des Underlying Events für viele Analysen nötig ist.

Ein Colour-Reconnection-Modell wurde implementiert. Es greift in den Hadronisierungs-Prozess ein, indem es die Neubildung sogenannter Cluster ermöglicht. **Herwig++** benutzt für die Hadronisierung ein Modell, in dem die Partonen, die im Wesentlichen vom Parton-Schauer hervorgebracht wurden, zu farbneutralen Objekten, den Clustern, zusammengefasst werden. Diese können als hoch angeregte hadronische Zustände angesehen werden. Die Cluster zerfallen letzten Endes (isotropisch) in Mesonen und Baryonen. Das unveränderte Hadronisierungs-Modell fasst Partonen zu Clustern zusammen, zwischen denen eine Farbverbindung besteht. Der Ursprung dieser eindeutigen Zuordnung liegt darin, dass **Herwig++** den Limes vieler Farbladungen benutzt. Dadurch entsteht ein eindeutiger Farbfluss im Event.

Das Colour-Reconnection-Modell sorgt nun dafür, dass auch solche Partonen zu Clustern verbunden werden können, die zwar nicht farbverbunden sind, deren Raumzeit-Abstand jedoch klein ist. Diese Idee erscheint recht sinnvoll, wenn bedacht wird, dass Quarks tatsächlich nur in drei Farbladungen auftreten.

Um die Partonen mit der nötigen Raumzeit-Information auszustatten, wurde ein Raumzeit-Modell zusammengestellt und implementiert. Dieses Modell ist imstande, mit vielen Parton-Parton-Wechselwirkungen auf eine sinnvolle Art umzugehen. Dabei wird eine Abschätzung für eine räumliche Parton-Verteilung innerhalb des Hadrons hinzugezogen.

Eine detaillierte Analyse des Teilchen-Flusses in hadronischen W -Paar-Zerfällen wurde durchgeführt. Diese Observable ist ausführlich von den LEP-Kollaborationen untersucht worden, da eine quantitative Abschätzung des Colour-Reconnection-Effekts den systematischen Fehler in der W -Massen-Bestimmung reduzieren kann. In dem untersuchten Prozess zerfallen beide W -Bosonen hadronisch. Die beiden Zerfallsorte sind im Allgemeinen zu weit voneinander entfernt, als dass Interferenz-Effekte in der perturbativen Phase wahrscheinlich sind. In der nicht-perturbativen Phase ist jedoch ein Überlapp der beiden Hadronisierungs-Regionen wahrscheinlich. Die Simulation *ohne* Colour-Reconnection weist systematische Abweichungen auf. Es wurde beobachtet, dass Colour-Reconnection nur leichte Veränderungen in dieser Observablen verursacht. Die *a priori* vorhandenen Abweichungen konnten mit diesem Colour-Reconnection-Modell nicht kompensiert werden. Das Modell konnte daher nicht, wie geplant, an die Daten angepasst werden.

Der Ursprung dieser Abweichung von den experimentell gemessenen Daten wurde im Parton-Schauer vermutet. Deshalb wurde untersucht, welche Folgen eine stufenweise Unterdrückung großwinkliger Emissionen im Parton-Schauer auf die Teilchen-Fluss-Observable hat. Eine Veränderung konnte jedoch nicht beobachtet werden.

Um dieses negative Ergebnis zu verstehen, wurde eine leichte (und doch gravierende) Veränderung im Colour-Reconnection-Algorithmus erprobt. Ein alternatives Modell wurde implementiert, welches nach einem anderen Prinzip funktioniert: Es sorgt dafür, dass vorzugsweise Partonen zu Cluster kombiniert werden, die sich nahe im *Impulsraum* befinden. Das führt zu einer Verringerung der mittleren Cluster-Masse. Tatsächlich konnte der Teilchen-Fluss mit Hilfe dieses Modells besser beschrieben werden.

Zum Schluss wurde die Auswirkung beider Modelle auf die Simulation des Underlying Events in Hadron-Kollisionen untersucht. Die Analyse basiert auf Daten des CDF-Experiments am Tevatron. Da diese letzte Analyse jedoch nicht sehr detailliert ausfallen konnte, dient diese Analyse lediglich als Ausblick. Im Speziellen wurde die geladene Multiplizität $\langle N_{\text{ch}} \rangle$ und die Summe der skalaren Transversal-Impulse p_{\perp}^{sum} in der sogenannten “transverse”-Region untersucht. Diese Region im η - ϕ -Raum wird mit Hilfe des härtesten Jets im Event definiert. $\langle N_{\text{ch}} \rangle$ und p_{\perp}^{sum} in diesem Bereich können als Maß für die Underlying-Event-Aktivität benutzt werden.

Kurz gesagt, sowohl $\langle N_{\text{ch}} \rangle$ als auch p_{\perp}^{sum} werden durch das *raumzeit-basierte* Colour-Reconnection-Modell erhöht. Das geschieht gleichmäßig und unabhängig vom Transversal-Impuls des härtesten Jets. Darüber hinaus lässt sich sagen, dass die Auswirkungen dieses Colour-Reconnection-Modells auf die beiden Observablen korreliert zu sein scheint.

Demgegenüber erzielt die Underlying-Event-Simulation mit Hilfe des *impuls-basierten* Colour-Reconnection-Modells aussichtsreichere Ergebnisse. Soweit sich das zu diesem Zeitpunkt sagen lässt, wird die Beschreibung der experimentellen Daten infolge dieser Art von Colour-Reconnection verbessert. Zudem ist die Auswirkung auf $\langle N_{\text{ch}} \rangle$ und p_{\perp}^{sum} nicht so stark korreliert wie im raumzeit-basierten Modell.

Abschließend lässt sich sagen, dass diese Arbeit als Ausgangspunkt für weitere Colour-Reconnection-Studien dient. Die Programme, die im Rahmen dieser Arbeit zur Verfügung gestellt werden, bieten die Möglichkeit, die Vorhersagekraft von **Herwig++** zu verbessern. Beide Modelle sind jedoch noch nicht ohne Weiteres benutzbar. Mit Hilfe weiterer Teststudien wird sich zeigen, ob eines der Modelle letzten Endes in Zukunft zum Standard-Repertoire von **Herwig++** gehören kann. Das impuls-basierte Modell scheint dabei besondere Aufmerksamkeit zu verdienen – obwohl es nur ein Nebenprodukt dieser Arbeit ist.

Danksagung

Zunächst möchte mich bei Herrn Prof. Dieter Zeppenfeld für die Betreuung meiner Arbeit sowie für seine Unterstützung darin bedanken. Ich konnte sehr viel von ihm lernen, nicht nur während meiner Zeit als Diplomand in seiner Gruppe. Ich danke ihm auch für seine Korrekturvorschläge für diese Arbeit.

Mein besonderer Dank gilt Herrn Dr. Stefan Gieseke, der diese Arbeit mitbetreut hat. Von ihm konnte ich in zahlreichen Gesprächen sehr viel lernen. Besonders dankbar bin ich ihm dafür, dass er sich immer Zeit für mich genommen und mich in meiner Arbeit stets unterstützt und ermutigt hat. Ich danke ihm außerdem sehr dafür, dass er mir die Möglichkeit gegeben hat, am *MCnet meeting* am CERN teilzunehmen.

Herrn Prof. Günter Quast danke ich herzlich für seine Bereitschaft, das Korreferat zu übernehmen.

Meinen besonderen Dank verdienen auch Ken Arnold, Ramona Gröber, Christian Hangst, Franziska Schissler, Andrzej Siodmok und Jorinne Sturm für das Korrekturlesen dieser Arbeit.

Bei allen Instituts-Mitgliedern möchte ich mich für die freundliche und hilfsbereite Atmosphäre bedanken. Besonders hervorheben möchte ich dabei Simon Plätzer, der mir in vielen technischen, aber auch in physikalischen Angelegenheiten weiterhelfen konnte.

Ich danke außerdem Mike Seymour dafür, dass er mir bei Problemen mit HERWIG geholfen hat.

Schließlich bedanke ich mich bei meiner Mutter für ihre Unterstützung und ihren Rückhalt während meines gesamten Studiums und viel mehr noch dafür, dass sie mir ein Studium überhaupt ermöglicht hat.

Zu guter Letzt danke ich Jorinne für ihre Liebe und Unterstützung.